Hybrid heterostructures and devices based on 2D layers and wide bandgap materials

Zhenping Wu[a*], Wenjing Jie[b], Zhibin Yang[c], Jianhua Hao [d,e,*]

[a] *State Key Laboratory of Information Photonics and Optical Communications & School of Science, Beijing University of Posts and Telecommunications, Beijing, 100876, P. R. China.*

[b] *College of Chemistry and Materials Science, Sichuan Normal University, Chengdu, 610066, P. R. China.*

[c] *Center for Terahertz Waves and College of Precision Instrument and Optoelectronics Engineering, Tianjin University, Tianjin, 100876, P. R. China.*

[d] *Department of Applied Physics, The Hong Kong Polytechnic University, Hung Hom, Hong Kong P. R. China.*

[e] *The Hong Kong Polytechnic University Shenzhen Research Institute, Shenzhen, 518057, P. R. China*

*Corresponding authors. Email: zhenpingwu@bupt.edu.cn (Z.P. Wu); jh.hao@polyu.edu.hk (J.H. Hao)

Abstract:

With the further development of Moore's law, the process nodes of integrated circuit have reached 7 nm or even smaller size. In addition to the significant increase in cost, when the scale continues to shrink, there will inevitably be short channel effect. For example, because of tunnelling and reduction in the separation of drain and barrier, the channel will be difficult to be completely turned off, thus reducing the switching performance of the device. Significant efforts have been dedicated for developing next-generation devices and applications to overcome these obstacles. The emerging van der Waals (vdW) heterostructures, where two-dimensional (2D) materials are physically layer-by-layer stacked without constraints on the chemical bonding and interfacial lattice matching, have offered an alternative platform in nanoscale electronic and optoelectronic applications. Beyond all 2D materials based vdW heterostructures, the concept could be extended to integrate 2D materials with conventional wide bandgap (WBG) functional materials. Here we summarize recent developments of 2D/WBG hybrid heterostructures starting from the integration process and working principle. Then, we highlight the functions and device applications of 2D/WBG hybrid heterostructures, including ferroelectric gating, piezoelectric strain engineering, photodetector, field effect transistor, photocatalyst, and gas sensor. Finally, we provide a brief discussion on the perspectives and challenges in this exciting field.

1. Introduction

Two-dimensional (2D) materials are atomically thin sheets with layered structure, where the neighbor layers are connected by van der Waals (vdW) forces and intralayer is constructed by covalent bonds. The rise of 2D materials started from the discovery of graphene in 2004 via a mechanically exfoliated method by Geim *et al* at Manchester University [1]. With a structure of single carbon atom layer via sp^2 hybridized, graphene presents excellent properties, including pronounced carrier mobility, large theoretical specific surface area, high electrical conductivity and superior thermal conductivity, leading to an increased attention of all 2D materials [2]. To overcome the obstacles resulted from the absence of a bandgap in graphene, a large variety of emerging 2D materials with prominent physical and chemical properties have subsequently been recognized, including transition metal dichalcogenides (TMDs) [3-5], phosphorene [6-8], hexagonal boron nitride (h-BN) [9], and so on. 2D materials are expected to possess intriguing electrical, thermal, optical and mechanical properties due to their unique structure with high surface-bulk ratio. In particular, there is an increasing interest in assembling different 2D materials together to form heterostructures via vdW interactions. Such vdW heterostructures originally refer to physically stacking 2D materials layer-by-layer by weak vdW force ($6.409 \times 10^{-21} \sim 1.122 \times 10^{-20}$ N·m) with unprecedented performance and functionality.[10] Compared with the conventional superlattices and heteroepitaxy structures which have been extensively studied in modern semiconductor technology, the past decade has witnessed even more remarkable rapid progress on vdW heterostructures in developing next-generation

stretchable, implantable, portable, and wearable electronics and optoelectronics, owing to their absence of constraints on the chemical bonding and interfacial lattice matching [11-13]. Up to now, the vdW heterostructures are not limited to interlayer interactions within 2D layered materials (2D/2D), which provides considerable freedom to integrate disparate materials with distinct dimensionality [14]. The emergence of mixed-dimensional vdW heterostructures including 2D/0D (quantum dots) [15], 2D/1D (nanowires) [16], and 2D/3D (bulk) [17] with both structural and material varieties have paved the way towards designing promising applications, including light-emitting diodes (LEDs), optical modulators, transistors, photodetectors, *etc*.

In particular, the availability of mixed-dimensional vdW heterostructures involving functional materials such as metals, semiconductors, and insulators (including dielectrics, ferroelectrics, *etc.*) could expand both the fundamental research and practical applications of 2D materials. Among these functional materials, wide bandgap (WBG) materials, which possess an energy bandgap (E_g) typically larger than 3 eV, are preferred over narrow band materials for some electronics applications, because the large energy separation between conduction and valance bands allows the device to potentially operate at elevated temperatures and high voltages. Traditional dielectrics such as SiO_2 (E_g: ~ 9 eV), HfO_2 (E_g: ~ 5.9 eV) and Al_2O_3 (E_g: ~ 7.4 eV) have been routinely employed as gate materials integrated into electronic devices. In this review, we mainly focus on WBG semiconductors and ferroelectrics incorporated with 2D layers. Fig. 1 illustrates the schematic band diagram for common 2D materials, WBG semiconductors and ferroelectrics. Among them, ferroelectric materials possess the

characteristics of high dielectric permittivity, spontaneous polarization, large residual polarization and strong reverse piezoelectric effect, thus enabling wide application prospects in many fields, such as ferroelectric field effect transistor (FET), non-volatile memory, piezoelectric transducer, pyroelectric infrared detection, acoustic wave sensor and so on [18, 19]. It should be pointed out that ferroelectrics also possess piezoelectricity due to their non-centrosymmetric structure. Thus, both piezoelectric strain and ferroelectric gating can act as external perturbations to change the interface charge and further *in-situ* modulate the physical properties in 2D materials [20]. On the other hand, WBG semiconductors with large E_g could enable high breakdown electric field and short-wavelength emission, which may offer exciting device opportunities in high-power electronics, ultraviolet (UV) photodetectors, blue and UV LEDs and laser diodes [21]. Table I summarizes basic physical properties of typical 2D materials with monolayer and single-crystal WBG semiconductors, including bandgap, dielectric constant, breakdown electric field, electron mobility and thermal conductivity for comparison [21-23]. It is known that the realization of high-brightness blue LEDs using GaN-based materials in 1994 had inspired luxuriant research attentions for WBG semiconductors [24]. Commercial power devices based on SiC including metal–oxide–semiconductor field-effect transistors (MOSFETs) and Schottky-barrier diodes had been applied in industrial energy saving applications. With a larger critical field strength, SiC power switching devices offer significant advantages with much lower on-state losses and switching losses. In addition, ZnO is considered as the potential material for UV LEDs because of its high exciton binding energy (~ 60 meV) [25]. Very recently,

Ga_2O_3 is also emerging as a new class of WBG semiconductors with an ultrahigh breakdown field ~ 8 MV/cm and high-quality native substrates available up to 6 inches. The incredibly high breakdown field strength of Ga_2O_3 is 2 times higher than that of SiC and GaN, and 26 times higher than that of Si. Hence, Ga_2O_3 represents a strong candidate for power switching applications due to its enhanced Baliga figure-of-merit (FOM) [26]. The temperature has an important impact on semiconductors. First, the concentration of intrinsic carriers in semiconductors is exponentially dependent on the temperature. Secondly, the thermionic leakage increases with temperature as the carriers gain more thermal energy. Furthermore, the carrier mobility of semiconductor decreases due to the increased thermal vibrational energy and lattice scattering. Thus, the commercially silicon-based devices fail to work at high temperature due to some underlying mechanisms such as increased leakage currents, irreversible thermal damage, decreased electron mobility and so on. In contrast, with a wider E_g, the WBG semiconductors could retain low intrinsic carriers' concentration even at a higher temperature, which reduces the leakage current in the corresponding devices, making them become promising candidates for high-temperature electronics and optoelectronics (e.g., operation temperature $T > 200$ ºC) without any cooling system. However, there are some barriers to be overcome in those WBG semiconductor-based devices for further development. For instance, according to the fundamentals of doping effect on WBG materials in semiconductors physics, heavily doping could result in a shrink of E_g, while lightly doping could act as donors or acceptors. In WBG semiconductors, owing to their large E_g, some of the intentionally doping ions only

generate deep donor/acceptor level within energy bandgap with a large ionization energy. Therefore, the ionization efficiency in WBG semiconductors is reduced, which simultaneously reduces the possibility of modifying n-type or p-type semiconductor conductivities. Moreover, owing to the presence of oxygen vacancies, ZnO and Ga_2O_3 are intrinsic n-type semiconductors and lack of p-type doping under most conditions, thus hampering their PN homojunction construction. In the meantime, due to the large lattice mismatch and the formation of rotation domains, there are plenty of dislocations and defects in the heterojunction, resulting in an extremely large leakage current with non-ideal performance. Thus, 2D/WBG vdW heterostructures could overcome the constraint of lattice-matching and provide not only flexibility in constructing hybrid structure with diverse material arrangement, but also novel functions that conventional devices have inadequate capability to be demonstrated.

Although there are many reviews providing a general overview of vdW heterostructures and applications [12, 27-29], there has been no specific summary article focusing on hybrid heterostructures based on 2D layers and WBG materials. It is imperative to give an overview on the latest development of the particular nanoscale structures and their devices by considering the significance and rapid progress of this research field. Therefore, we will firstly summarize the integration methods for 2D/WBG hybrid heterostructures and their energy band alignment in this review article. Subsequently, we will overview the functions and emerging applications of some typical hybrid heterostructures based on 2D/WBG functional materials, including ferroelectric gating, piezoelectric strain engineering, photodetectors, FETs,

photocatalyst, and gas sensors. At last, we will conclude the article with perspectives and it is hoped to provide a guide for further development.

2. Integration methods and principle

2.1 Integration of 2D/WBG vdW heterostructures

The reliable integration techniques for 2D/WBG vdW heterostructures are of great significance for further study and device demonstration. Currently, mechanical transfer and direct synthesis through bottom-up methods are commonly used to achieve 2D/WBG heterostructures [12, 27, 30]. Thanks to the vdW interactions between neighboring layers and free of dangling bonds, 2D vdW heterostructures can be easily constructed by artificially stacking layered nanosheets in arbitrary order, which are mechanically exfoliated from their bulks. Up to now, a large number of 2D/WBG heterostructures, such as $MoS_2/BaTiO_3$, MoS_2/ZnO, WSe_2/Ga_2O_3, have been produced by this manual stacking method [31-35]. Particularly, Jeon *et al*. have fabricated a 2D-1D diode by attaching mechanical exfoliated black phosphorus (BP) nanosheet onto chemical vapor deposition (CVD) grown ZnO nanowire with the assistance of a sticky polydimethylsiloxance (PDMS) stamp (Fig. 2a) [34]. The obtained heterostructure preserves the pristine electronic properties of both BP and ZnO, which is one of main advantages of mechanical transfer method. However, the interface of the heterostructure may be contaminated by the chemical residue during the transfer process, which could largely bring down the quality of the heterojunction devices. Meanwhile, the lateral size is not scalable and controllable due to the feature of mechanical exfoliation method, which limits its further application in practical devices.

In comparison with mechanical transfer, direct synthesis methods with bottom-up strategy, such as CVD and physical vapor deposition (PVD), have proved to be powerful tools in preparing large-area 2D materials and heterostructures [27, 36]. Recently, a number of 2D/WBG heterostructures, such as graphene/Ga_2O_3, MoS_2/GaN, $MoSe_2$/GaN and so on, have been realized by CVD method [37-41]. The lateral size, morphology and layer number can be adjusted by the growth parameters, such as growth temperature, rate of gas flow, volume of precursors. For example, Chen *et al*. have grown wafer-scale, atomically thin $MoSe_2$ thin films on both GaN single crystalline substrate and p-GaN thin film by CVD, respectively [40]. The morphology of the obtained $MoSe_2$ film can be controlled by the growth position inside the CVD tube (Fig. 2b). Continuous $MoSe_2$ film with full coverage on 1 cm × 1 cm GaN substrate can be obtained (Fig. 2c). Besides, multi-layered 2D/WBG heterostructure can also be obtained by CVD. As shown in Fig. 2d, monolayer/few-layer MoS_2/WSe_2/n-GaN heterostructure was constructed by directly depositing MoS_2 film on WSe_2/n-GaN, exhibiting sub-monolayer domains in monolayer MoS_2 and uniform surface in few-layer MoS_2, respectively [41]. Currently, CVD is still the most commonly used technique to synthesize large-size 2D materials. However, the high reaction temperature and long fabrication time make the synthesis process of some heterostructures difficult. Meanwhile, some chemically sensitive materials, such as BP, are not suitable to be prepared by CVD [36].

Pulsed laser deposition (PLD) is widely used in synthesizing complex oxide thin films, heterostructures and superlattices in previous works [42, 43]. Thanks to the

ability of precisely controlling on thickness and stoichiometric transfer from target to substrate, PLD has been employed to grow wafer-scale 2D materials as an alternative method to CVD in recent years [44-47]. Compared to CVD, PLD is free of potentially dangerous chemical precursors. By directly depositing 2D materials on WBG single-crystal substrate, 2D/WBG heterostructure can be readily constructed [48-51]. Serna *et al*. reported that 1-10 layers of MoS_2 film with high uniformity were deposited on various substrates including single-crystal sapphire and quartz, polycrystalline HfO_2 and amorphous SiO_2 by PLD without any surface treatment, [48]. As sulfur is easily losing during the deposition, more sulfur content should be incorporated in the target. Therefore, to achieve the stoichiometric growth, the target composition was controlled at 1:1 of MoS_2/S. As shown in Fig. 2e, the MoS_2 film is fully covered on sapphire substrate with lateral size of 50.8 mm, resulting in wafer-scale of MoS_2/Al_2O_3 heterostructure. The layered structure of the film was verified by the cross-sectional TEM (inset of Fig. 2e). Furthermore, 2D MoS_2/GaN was realized by PLD with target composition 1:4 of Mo:S (Fig. 2f) [49]. The as-obtained heterostructure exhibits large area and good crystallinity as well, making it promising for developing high performance electronic and optoelectronic devices.

Another important issue needed to be considered is the interfacial contaminates of vdW heterostructures, which are mainly determined by the transfer methods. In general, the mechanical assembly of 2D materials can be achieved via either wet-transfer or dry transfer technique. The wet-transfer method is usually assisted by a handling layer of PMMA, which is also required to be removed in acetone after the integration [52]. The

residues induced by the dissolution of PMMA will be left on the surface of 2D materials. On the other hand, the dry transfer method is usually carried out by a pick-and-lift technique with the assistance of PDMS stamp, which could provide a cleaner interface compared with the wet-transfer. However, these polymeric stamps will also unintentionally absorb some contaminated materials, which result in the formation of protrusion-like impurities [53]. Recently, a roll-to-roll (R2R) dry transfer technique has been developed for constructing heterostructures based on CVD grown graphene [54]. By controlling the experiment conditions, such as linear film speed, separation angle and guiding roller diameter, the R2R method could provide clean, highly coverage graphene heterostructure.

In summary, 2D/WBG vdW heterostructure could be effectively realized by various techniques. Among them, mechanical transfer could largely preserve the pristine physical properties of 2D materials, which is suitable for fundamental study. On the other hand, CVD and PLD methods enable the scalable synthesis of 2D/WBG heterostructures, offering the great possibility for future research towards practical applications.

2.2 Electronic band alignment of 2D/WBG

It should be noted that, to a large extent, the electronic band structure at the interface dedicates the carrier transport characteristics, threshold voltage stability, field effect mobility, and performance reliability [55]. The band alignments are mainly determined by the energy difference between conduction band (E_C) and valence band (E_V) extrema in the constituent layers. The band offsets at interfaces are the key

components that govern the barrier height (Φ_B) for carrier transport due to the bandgap discontinuities across the interfaces. The Φ_B could be predicted by taking into account of Anderson's rule [56] and quantum dipole theory [57] for semiconductor heterojunctions and Schottky–Mott rule for metal/semiconductor junctions [58-60]. Different fabrication techniques, growth mechanisms and post-treatments may vary chemical bonding and band alignment at the interface [61]. Moreover, the charge carrier injection from WBG materials towards 2D layers could also affect the interfacial band offset and Φ_B. 2D materials possess varying bandgaps from gapless graphene [62], semimetals WTe_2 [63-65] and 1T'-$MoTe_2$ [66, 67], semiconducting BP [68-71], InSe [72-74], MoS_2 [75, 76], WSe_2 [77, 78], to insulating h-BN [79]. To realize high performance devices based on 2D/WBG vdW heterostructures, rational selection of materials with suitable bandgap and band alignment is of vital importance. Fig. 3(a) shows a schematic atomic structure of the 2D/WBG vdW heterostructure. For gapless graphene combined with WGB materials, Ohmic contact (Fig. 3b) or Schottky barrier junction (Fig. 3c) could be formed, depending on the magnitudes of work function and electron affinity from the contacted metal and semiconductor. For 2D semiconducting materials, considering the difference between bandgap and electron affinity, three configurations of vdW heterostructures are constructed, namely type I, II, and III (Fig. 3d-e). In type I band alignment, carriers could be spatially confined in quantum wells to promote electron-hole recombination efficiency, which is commonly used in LEDs and lasers [80-82]. The device performance could be further boosted by building multiple quantum wells [83]. In type II band alignment, larger band offset on either E_V

or E_C is obtained, resulting strong carrier confinement near the interface. When the 2D/WBG vdW heterostructure is formed, there usually exists a large charge density gradient. Therefore, some of free electrons from the donor impurities in n-type region could migrate across the interface and fill up the holes in p-type region, which consequently produce negative ions in p-type region while positively charged ions are left in n-type region. Such charge transport of electrons and holes across the heterostructure is known as diffusion. The presence of impurity ions on both sides of the heterostructure then develops a built-in electric field to prevent more carriers from crossing the interface. Generally, there are two major mechanisms for the diffusion process, namely interstitial and substitutional, where the atoms of diffusing impurities can either exist on a lattice site as a substitutional atom or as an interstitial. Other possible mechanisms including the ring mechanism, interstitialcy, and random jump should also be considered to understand the diffusion process. Then, a potential barrier will eventually form under equilibrium conditions to prevent the majority carrier flowing. The intrinsic built-in field emerges as an attractive strategy to hinder the recombination of the photoexcited carriers and hence improves the performance of optoelectronic devices, including photodetector, phototransistor and photocatalyst [84]. When a forward bias is applied, the total current will be the sum of the electron and hole currents, including both drift and diffusion currents. The applied electric field could not only promote the separation of the electron-hole pairs, but also increase the possibility to cause the failure in interconnect parts within the device. For instance, carriers could flow through potential barrier under electric field due to the existence of

defects and dislocations near the interface. Benefiting from larger band offsets, type III band alignment is particularly suitable to meet the requirement of tunneling FETs, where tunneling current density could be highly increased [85]. Theoretical calculations on the band alignments for 2D materials based vdW heterostructure, including MoS_2/SiC, BP/AlN, MoS_2/GaN, etc. were performed by many groups [84, 86-90]. Fig. 4 presents a periodic table of heterojunction type as a valuable guidance for future hybrid heterostructure fabrication [88]. The WBG materials could also be selected as the gate dielectric for fabricating MOSFET, metal-insulator-semiconductor field effect transistor (MISFET). Under this circumstance, a sufficient $\Phi_B > 1$ eV is highly preferred to block the leakage current between the channel 2D layer and WBG insulating gate material [91, 92]. To experimentally determine the band alignment for 2D/WBG vdW heterostructures, both bandgap and band offsets should be measured. Ultraviolet-visible (UV-Vis) spectroscopy and reflection electron energy loss spectroscopy (REELS) techniques are two straightforward routes to investigate the bandgaps for WBG materials, while the magnitude of bandgaps for 2D materials particularly with direct bandgaps is usually determined by using photoluminescence (PL) measurement. Meantime, the band offsets could be obtained using X-ray photoelectron spectroscopy (XPS) or ultraviolet photoelectron spectroscopy (UPS) to check the chemical bonding states. Then the valence band offsets (ΔE_V) and conduction band offsets (ΔE_C) could be extracted based on Kraut's method [93].

3. Hybrid heterostructures and devices based on 2D/ferroelectrics

3.1 Ferroelectric gating based device

Owing to the atomically thin structure, the physical properties of 2D materials could be effectively modulated by the interfacial electrostatic gating [20, 94]. The gate electric field could effectively control electron propagating along the source-drain channels. Compared to conventional SiO_2 gate dielectric, the polarization resulted from ferroelectric materials typically could reach one order of magnitude higher. $Pb(Zr,Ti)O_3$ (PZT), with a relatively large remnant polarization 50~100 μC cm^{-2}, is commonly integrated in hybrid heterostructure as the ferroelectric materials. In 2009, Hong and co-workers first reported FETs based on few-layer graphene/PZT hybrid heterostructures, in which PZT film was utilized as the ferroelectric gate oxide and graphene as the channel material [95]. The obtained FET exhibited a n-type conductance with a carrier density of 2.4×10^{12} cm^{-2} and a significant enhanced mobility up to 7×10^4 $cm^2/(Vs)$. The obtained mobility is much higher than that of graphene/SiO_2 FET. In 2011, Zheng *et al*. reported large size monolayer and bilayer graphene/PZT FETs fabricated by CVD [96]. The device could operate at an ultra-low voltage lower than ±1 V, with an ON/OFF ratio over 10 times and a maximum doping over 10^{13} cm^{-2}. Moreover, the non-volatile memory based on graphene/ferroelectric was studied by utilizing the ferroelectric nonvolatility characteristic. A series of ferroelectric materials have been employed in the graphene-based non-volatile memory, from inorganic PZT, $(1-x)[Pb(Mg_{1/3}Nb_{2/3})O_3]$-$x[PbTiO_3]$ (PMN-PT) to organic ferroelectric poly(vinylidene fluoride-co-trifluoroethylene) (PVDF-TrFE) [97-100]. Beyond graphene, a series of newly discovered 2D materials have been reported to be

integrated with ferroelectric materials to improve their physical or chemical properties in order to achieve novel performance. Similar to graphene, non-volatile memories have been achieved based on TMDs, such as MoS_2 and WSe_2 [101, 102]. Furthermore, ultrasensitive and broadband photodetector based on MoS_2 was achieved by ferroelectric gating [103]. By utilizing the ferroelectric $LiNbO_3$ (LNO) substrate, monolayer MoS_2 can be well templated because the MoS_2 layer prefers to grow on the ferroelectric substrate where the polarization pointing to "up" [104].

In non-volatile memory, graphene typically shows *p*-type transport properties rather than intrinsic bipolar properties. Thus, some strategies have been proposed to tune the transport characteristics of graphene. By ferroelectric gating, a complete conversion from *p*-type to bipolar and further into *n*-type for graphene was achieved in vacuum condition [105]. As shown in Fig. 5a, CVD-grown single-layer graphene-based FET is fabricated with the pulsed laser deposited ferroelectric PZT thin film as the gate dielectric and the conductive $SrRuO_3$ layer on $SrTiO_3$ substrate as the gate electrode. The carrier type and density in the graphene layer can be controlled by the ferroelectric polarization arising from the underlying PZT. Through a pre-stimulation of the pulse voltages higher than the coercive voltages of the PZT thin film, the carrier type of graphene can be effectively tuned from *p*- to eventual n-type, as shown in Fig. 5b. The polarization of PZT can be completely switched and can be retained by the initial pulse voltages larger than the coercive voltage. The switched polarization can tune the initial carrier type of graphene and further change the device from *p*- to *n*-type.

The vertical graphene FETs show intriguing properties compared to traditional

graphene-based lateral FETs. Inspired by ferroelectric tunnel junctions (FTJs), graphene based FTJs have been fabricated by using an ultrathin ferroelectric $BiFeO_3$ (BFO) film as the tunnel barrier layer [106]. It is reported that the graphene based FTJs possess ultrahigh current on/off ratio up to 7×10^7 by switching the ferroelectric polarization of the BFO thin film. Moreover, MoS_2-based FTJs were proposed based on ferroelectric $BaTiO_3$ (BTO) [31]. The electronic and transport properties of MoS_2 can be modulated by the giant tunneling electroresistance effect from the heterostructure of MoS_2/BTO, as shown in Fig. 5c. The resistance ON/OFF ratio can be improved up to 10^4 at the read voltage of 0.1 V if the whole area of the BTO films covered by the MoS_2 flake is uniformly poled, as shown in Fig. 5d. It was proposed that the observed tunnelling effect stems from the reversible accumulation and depletion of the majority carriers in the MoS_2 layer due to the ferroelectric switching. The 2D materials based FTJs provide a new strategy to improve the transport properties of the 2D materials.

3.2 Piezoelectric strain engineering based device

Instead of modulation from the ferroelectric, the properties of 2D materials can be modulated by the interfacial strain from the underlying substrate owing to the atomically thin structure. Strain engineering is proposed to open a gap in graphene or tune the magnitude of bandgap in 2D semiconductors. The electric band structure of 2D materials can be controlled by the external strain modulations in real-time and reversible ways. Actually, the strain provided by the piezoelectric substrates is biaxial in nature, which is different from conventional uniaxial strain via bending or stretching

[107, 108]. Nowadays, ferroelectric PMN-PT single crystal substrate has been extensively utilized for strain engineering which can provide the largest available piezoelectric coefficients d_{33} up to ≈2500 pC N^{-1}. It was reported that biaxial strain can generate more remarkable changes in band structure compared to uniaxial one, especially the dramatic increase in band gap and the enhanced PL for trilayer MoS_2 under compressive biaxial strain [109]. Generally, the uniaxial strain can be provided to 2D materials by bending or stretching underlying flexible substrates [110, 111]. Such uniaxial strain can typically induce a red shift in wavelength and decrease in intensity of PL for monolayer MoS_2. Comparatively, by utilizing biaxial piezoelectric strain triggered from PMN-PT, a blue shift and enhanced intensity can be achieved in trilayer MoS_2 [109], where real-time modulating band energy and optical properties of trilayer MoS_2 are demonstrated by piezoelectric PMN-PT with top electrode of graphene. In this heterostructure, monolayer CVD-grown graphene and Au serve as the top and bottom electrode, respectively. External electric field was biased to the piezoelectric PMN-PT, as schematically shown in Fig. 6a. Then, the piezoelectric strain generated by the PMN-PT can be delivered to the above MoS_2 trilayer. The tunability of the indirect band gap by biaxial compressive strain is much higher than above mentioned one of the direct bandgap through uniaxial tensile strain. A blue shift in bandgap of 300 meV/% strain was reported for the trilayer MoS_2 by a piezoelectric substrate. Furthermore, it is important that the piezoelectric biaxial strain can enhance the PL intensity (Fig. 6b), which can be well explained by the indirect-to-direct band gap transitions in trilayer MoS_2.

Moreover, by utilizing the piezoelectric PMN-PT, the controllable energy of single photon can be achieved from monolayer WSe_2 [112]. The single photon emitters (SPEs) can be fabricated by integrating PMN-PT with wrinkled monolayer WSe_2, as shown in Fig. 6c. The PL spectra of a SPEs can be effectively tuned by the applied electric field (Fig. 6d). The positive and negative electric fields can generate compressive and tensile strains, respectively, and further give rise to the observed red- and blue-shifts in the PL (Fig. 6e). The electric field from −20 to 20 kV/cm can modulate the energy of localized excitons up to 5.4 meV without degrading their PL intensity. Furthermore, when transferred the winkled WSe_2 monolayer onto PMN-PT (110), the piezoelectric biaxial strain up to ~0.15% can be delivered to the WSe_2 monolayer and reversibly tune the energy of localized excitons up to 18 meV. Thus, the studies of heterostructures based on 2D layers and piezoelectric provide not only a new way to understand the effects of biaxial strain on 2D materials but also new strategies to modulate the emission and single photon emission devices based on 2D materials.

4. Hybrid heterostructures and devices based on 2D/semiconductors

4.1 Photodetectors

Photodetectors have received huge attentions owing to their fascinating potential applications in modern society, such as monitoring, chemical/biological analysis, communication, healthcare, energy harvesting, etc. Thanks to their tunable work function, strong light–matter coupling and ultrafast carrier dynamics, 2D materials have provided new opportunities for broadband and high-speed detection with considerable quantum efficiency and sensitivity. The integration of 2D materials with WBG

semiconductors would therefore enable visible-blind or even solar-blind photodetection. Ideal photodetectors typically should satisfy the "5S" requirements, including fast speed, large signal-to-noise ratio, high sensitivity, good spectrum selectivity, and high stability. The existence of potential barrier and built-in field generated near the 2D/WBG interface could suppress the dark current and promote the photoexcited electron/hole pairs separation, which will meet the practical application requirement. Earlier results based on Schottky barrier junctions, such as graphene/ZnO [113], graphene/GaN [114, 115], graphene/SiC [116], graphene/Ga_2O_3 [37, 117, 118], and graphene/diamond [119], all exhibited considerable enhanced performance. For instance, Kong and co-workers reported a solar-blind photodetector based on graphene/Ga_2O_3 heterojunction [37]. The device presented an ultrahigh responsivity of 39.3 A/W and a detectivity D* of 5.92×10^{13} $cmHz^{1/2}W^{-1}$, which is superior to those previously reported Ga_2O_3 based photodetectors (Fig. 7a-c). Inspired by the pioneer work done by Konstantatos et al., a high gain photogating mechanism in hybridized graphene structures was proposed [15]. A hybrid GaN/graphene photodetector was fabricated by epitaxial growth of GaN on graphene. The built-in field at the interface separates the photoinduced electron-hole pairs, where electrons are trapped in GaN and holes are injected into graphene. This photogating effect could effectively modulate the Fermi level in graphene, resulting in a change of conductance. The device presented a high responsivity over 2 A/W under 10 $\mu W/cm^2$ and 365 nm light illumination (Fig. 7d-f) [115]. To further enhance the device performance, larger potential barrier especially type II band alignment is highly demanded. Researchers then turned to construct

2D/WBG p-n junctions other than Schottky barrier junctions by replacing graphene with other 2D semiconductors. MoS_2 flake could change from *n*-type to *p*-type semiconductor after SF_6 plasma treatment. Then a MoS_2/ZnO *p-n* junction was fabricated [32]. Compared to untreated *n*-MoS_2/ZnO heterojunction, the rectifying ratio is highly increased. The device demonstrates a strong 365 nm photoresponse with an external quantum efficiency ~ 52.7% and a fast response time of 66 ms. In particular, the ultraviolet photodetectors usually function in harsh environment, where a self-powered operation mode is more favored. Therefore, self-powered ultraviolet photodetectors based on MoS_2/GaN [120], WS_2/GaN [121], and MoS_2/Ga_2O_3 [122] vdW heterojunctions were reported. Fig. 7(g) shows the schematic illustration of the large scale WS_2/GaN vdW heterojunction. Fig. 7(h) shows that the responsivity and specific detectivity of the device can reach up to 226 mA/W and 4×10^{14} Jones, respectively, under 1 μW/cm^2 and 375 nm light illumination without applied voltage. Moreover, the obtained device could be used in the image applications with high resolution and high voltage contrast over 8×10^3 [121].

4.2 Field effect transistors

FETs are always regarded as the backbone for modern communication and information electronics. Since the atomic scale limit for Si microelectronics is approaching, the WBG semiconductors are considered as the complementary materials especially in those devices requiring high power density metrics. Meanwhile 2D materials possess high electron mobility and atomically thin structure, which is beneficial for fabricating high-speed transistors. Thus, the combination of 2D and WBG

semiconductors might enable FETs with multiple functionalities and overcome intrinsic restrictions. Various types of FETs including junction field effect transistor (JFET), barrisors, and metal–semiconductor field-effect transistor (MESFET), *etc.* could be designed based on the diversity of 2D materials and device structure. By integration of *p*-type BP nanosheets and n-type ZnO, Jeon *et al.* presented a JFET based on BP/ZnO vdW heterojunction [33]. The JFET showed considerable rectifying characteristics with a high ON/OFF ratio up to 10^4, ideality factor ~1.3, and switching dynamics at kHz. After analyzing temperature dependent current-voltage curves under reverse bias, the Φ_B was extracted to be approximate ~0.7 eV with a type-I band alignment. Later, an optimized JFET was constructed by integrating WSe_2 with Ga_2O_3 [34]. The device exhibited improved transfer characteristics with a pronounced high source-drain current ON/OFF ratio ~ 10^8, a reduced sub-threshold swing of 133 mV/dec and a threshold of -5.1 V. The electron mobility obtained could reach up to 4.3 $cm^2V^{-1}s^{-1}$ and the leakage current is extremely low (10^{-8} mA/mm under negative gate bias). More importantly, the three-terminal breakdown voltage was measured to be +144 V, indicating an opportunity for power amplifier applications (Fig. 8a-c).

The atomically sharp graphene/semiconductor interface has enabled a novel three-terminal FET named barristor, where the Schottky barrier height could be modulated by gate voltage. Followed by the first graphene/Si barristor demonstrated in 2012 [123], 2D/WBG semiconductor barristers including graphene/GaN, graphene/Ga_2O_3, graphene/ZnO, etc. were reported. Graphene/N-doped ZnO barristor was found to exhibit an enhanced stability with a ON/OFF ratio up to 10^7 [124]. Improved thermionic

emission current and reduced flicker noise were obtained in graphene/GaN barristor [125]. In particular, the graphene/Ga_2O_3 vertical barristor was reported to present a ON/OFF ratio of around 10^4 with a record breakdown field of 5.2 MV/cm, exceeding the theoretical breakdown limits of GaN and SiC (Fig. 8d-f) [126]. To date, most of the Ga_2O_3 based FETs operate in a depletion mode (D-mode), where negative gate bias is required to inhibit the short-circuit. To solve the problem, Kim and co-workers fabricated both D-mode and enhancement-mode (E-mode) MESFET based on mechanically exfoliated graphene/β-Ga_2O_3 hybrid heterostructures with single- or double- graphene gate architecture, as schematically presented in Fig. 8(g) [127]. Both D-mode and E-mode MESFETs showed excellent rectifying behaviours, with high ON/OFF ratio up to 10^7 and ideality factors of ~1.5. Compared to single-gated D-mode device, the obtained E-mode device showed a positive threshold voltage of +0.25 V and a low subthreshold swing of 68.9 mV/dec. Integration of E-mode and D-mode MESFETs enables first demonstration of an area-efficient logic inverter with a noble inversion functionality (Fig. 8hi).

It is reported that 2D materials could also serve as the heat-escaping channels to solve the self-heating problem in high power electronics and optoelectronics. By introducing few-layer graphene on top of the AlGaN/GaN transistors operating at ~ 13 W mm^{-1}, *in-situ* micro-Raman spectroscopy monitoring exhibited a ~20 °C temperature decrease near the hotspots, which could extend the device lifetime by an order-of-magnitude [128]. A BN/Ga_2O_3 vdW heterostructure based metal-insulator-semiconductor field-effect transistors (MISFET) is fabricated, showing a considerable

small leakage current and a large ON/OFF ratio [129]. Subsequent theoretical and experimental results indicate that the mechanically exfoliated h-BN could be used as the field plate to decreases the peak electric field near the drain edge. The peak electric field could be reduced from 7.3 MV/cm to 4.3-4.5 MV/cm, thereby strengthening the reliability of the device.

4.3 Photocatalyst

Semiconductor photocatalysts for direct water splitting may meet the long-term pursuit for large-scale, renewable, clean fuel production, where hydrogen and oxygen can be generated using solar energy. Considering the redox potentials for H^+/H_2 and O_2/H_2O, the semiconductor bandgap must be larger than 1.23 eV [130, 131]. To promote the photocatalytic activity, photoexcited charge separation efficiency should be improved. Rational design and fabrication of 2D/WBG vdW heterojunctions in a type-II alignment endowed with reasonable band offsets have provided an ideal strategy for the enhancement of electron-hole pair separation. Theoretical density functional calculation results had highlighted the important potential of MoS_2/AlN and MoS_2/GaN vdW heterostructures in photocatalytic water splitting and stimulated further research [84, 87]. Afterwards, Yang and co-workers proposed AlN/BP heterostructure photocatalyst for high efficiency water splitting [132]. They found a direct bandgap characteristic in AlN/BP heterostructure with a type-II band alignment, which is beneficial to facilitating the photocatalytic efficiency. With a similar mechanism, a 40% enhancement in photocatalytic degradation was observed in a type-II MoS_2/ZnO heterostructure [133]. Both spin–orbit coupling and interfacial engineering effect

exhibited prominent impact on the photocatalytic performance in WS_2/AlN and MoS_2/AlN hybrid heterostructures [134, 135]. Through remote N_2 plasma treatment, a nitridation interfacial layer was introduced in monolayer MoS_2/GaN heterostructure, resulting a significantly increased conduction band offset ~0.5 eV and carrier recombination was considerably inhibited. The electron accumulation capability in GaN is enhanced, leading to a superior hydrogen generation rate [136]. Very recently, a systematically study was performed on the interface interaction, charge transfer/separation and optical characteristics in monolayer MoS_2/SiC vdW heterostructure. It is revealed that MoS_2 could also act as a passivation layer to eliminate the surface state of SiC and further improve the photocatalytic activity [137]. To date, although most of the works have been done on the theoretical predictions, it is anticipated that the interfacial interaction between 2D materials and WBG semiconductors can give rise to more extraordinary devices.

4.4 Gas sensor

Due to the combustion of fossil fuels and other pollution emissions, toxic gases in the atmosphere would not only be harmful to mankind, but also cause acid rain after reaction with water. Therefore, it is necessary to develop gas sensors with high performance, low power consumption and high sensitivity. 2D materials are also regarded as promising potential for gas sensing devices owing to their large surface-to-volume ratio and high surface sensitivity [138-141]. There are still some drawbacks of pure 2D material based gas sensor, such as low sensitivity, slow response and weak recovery. Meanwhile, the energy band alignment of the vdW heterojunction could be

precisely designed by selecting suitable 2D and WBG materials with different band gaps and working functions, so as to optimize the gas selectivity and performance [142, 143]. In 2018, it was reported that *p-n* heterojunctions could be formed using MoS_2/ZnO hybrid heterostructure via a simple wet chemical method, as shown in Fig. 9a-c [144]. Compared to pure MoS_2 gas sensors, the hybrid sensor demonstrated a 3050% enhanced sensitivity to 5 ppm NO_2, 90% of full recoverability, an ultrafast response speed of 40 s, a low detection concentration of 50 ppb, and a reliable long-term stability over 10 weeks. Reddeppa and co-workers construct a H_2/H_2S gas sensor based on reduced graphene oxide (rGO)/GaN hybrid heterostructure [145]. The sensor performance could be significantly enhanced by 365 nm UV light, the photogenerated carriers in both rGO and GaN could be responsible for improved sensitivity. The response speed of the rGO/GaN sensor could be further improved by functionalized with Au nanoparticles [146]. Very recently, a hydrogen gas sensor based on reverse-biased MoS_2/GaN vdW heterojunction was fabricated using bottom-up magnetron sputtering method with a post sulfurization process [147]. Upon hydrogen exposure, the Φ_B near the MoS_2/GaN interface would be modified under the reverse bias, thus dramatically improved sensitivity with fast response. Moreover, strong temperature dependent of the device sensitivity is observed, with an increased temperature from 25 ^oC to 150 ^oC, and an enhanced sensitivity from 21% to 157% for 1% hydrogen. Considering that the high mobility and saturation velocity of two-dimensional electron gas (2DEG) formed in AlGaN/GaN heterostructure could in favor for the enhancement of sensitivity and broaden the gas selectivity, Triet et al. proposed a 2DEG Schottky

diode gas sensor based on rGO/ZnO/AlGaN/GaN hybrid heterostructure [148]. Herein, rGO/ZnO was engaged as the sensing material. The detectivity limit of the gas sensor could reach 120 ppb, with a sensitivity of 0.88~1.88 ppm^{-1} level for NO_2, SO_2, and HCHO. This work sheds the light for enabling precious control of the selectivity at different concentration levels for various gases. Inspired by the previous report, Bag and co-workers constructed a vertical heterostructure diode (VHD) based on rGO/AlGaN/GaN hybrid structure, allowing detection of NO_2, SO_2, and NH_3 gas concentrations down to 150 ppb as, shown in Fig. 9d-f [149]. They found that the Fermi level and the effective Schottky Φ_B could be altered. The variation of Φ_B depends on the type of gas molecules, resulting in a modulation of the forward bias current of the VHD. The observed higher sensitivity, fast response and ppb level detection could be attributed to the charge transfer process across the 2D/WBG heterojunction. Taking into account of WBG semiconductor' superior thermally and chemically stable, these 2D/WBG vdW heterostructures will offer an opportunity for developing high performance gas sensors.

5. Conclusions and perspectives

The booming development of studies on 2D materials have ignited great interests in investigating vdW heterostructures assembled by different materials. Among them, the integration of ultrathin 2D layers and WBG functional materials provide new promising candidates for electronic and optoelectronic applications. In this review, we systematically overview the synthesis methods and proof-of-concept device applications of 2D/WBG heterostructures. Both mechanical transfer and direct

synthesis by bottom-up techniques for realizing the heterostructure have been summarized. Meanwhile, the energy band alignment of typical 2D/WBG heterojunction is discussed as well. Moreover, the applications of 2D/WBG in ferroelectric gating, piezoelectric strain, FETs, photodetectors, photocatalyst and gas sensors are reviewed. A variety of hybrid heterostructures introduced in this review have demonstrated broad usage of 2D/WBG combinations, which are desirable for developing high performance practical devices.

Although vdW heterostructures between 2D materials have been intensively investigated for decades, the integration of 2D layers with WBG materials is still in an incipient stage. There are many challenges and opportunities available for both the fundamental study and real device applications of 2D/WBG heterostructures, which are briefly described as follows.

(i) Over the past decade, a large number of 2D materials with diverse properties have been discovered. Meanwhile, the number of WBG materials is also numerous in the previous study. Currently, the investigations of 2D/WBG mainly focus on the heterostructure based on graphene. There is relative few experimental study on integrating 2D TMDs with ZnO or GaN when considering the plentiful possible combinations of 2D and WBG materials. More research should be conducted to conceive and fabricate novel heterostructures composed of different 2D and WBG materials, which may result in some unexpected features and potential applications. For example, WBG semiconductors are ideal candidates for LEDs. Integrating 2D materials with WBG semiconductors would help to enhance the device's performance, and may

pave the route to realize deep UV LEDs.

(ii) Diverse 2D layered materials have been reported to possess piezo- or ferroelectric properties by theoretical predictions or/and experimental confirmations. Although a range of 2D materials have been integrated with ferro- and piezoelectric materials, WBG/2D ferro- or piezoelectric heterostructures have not yet been investigated experimentally up to now. The combination of 2D ferro- or piezoelectric materials with WBG functional materials may improve existing performance or generate new features for 2D materials and their devices based on the heterostructures, especially in nanoscale electronics and optoelectronics. Thus, investigation of WBG/2D ferro- or piezoelectric heterostructures is desirable for foundational research and practical applications. Such unique vdW heterostructures can provide a platform to investigate some intriguing effects associated with 2D domain patterns and piezoelectric charges.

(iii) The device applications of 2D/WBG heterostructure are mainly limited by the scalable synthesis of 2D materials. Although CVD and PVD have proved to be effective tools for preparing wafer-size 2D films, it is still much needed to improve the properties of the synthesized products in terms of uniformity, continuity, crystallinity and controllability. Additionally, the quality of the interface between 2D films and WBG functional materials plays a crucial role in achieving high-performance heterojunction device. The defects within interface of the heterostructure should be suppressed by adjusting the growth process and passivation treatment. Moreover, along with development of synthesis techniques, more complex 2D/WBG heterostructure with

multilayers could also be designed and realized, which is meaningful for designing multifunctional devices in the future. Also, it is found that the morphology of 2D materials is linked closely with their charge density, electronic density of state and lattice symmetry, resulting in variations of the electrical and optical properties. While, the morphology of 2D materials could be varied owing to the thermal motion, lattice growth kinetics and transfer techniques. The formation mechanism, design strategies, and structural modification of 2D materials have been extensively studied recently. For example, the morphology of TMDs in hybrid heterostructure normally shows triangular form as shown in Fig. 10a,b. Moreover, according to the different configurations, the morphology of 2D materials in hybrid heterostructures can be classified into grain boundaries, atomic defects, edge structures, *etc*. (Fig. 10c,d,e). Thus, the modulation of the 2D/WBG heterostructure performance based on morphology should be further studied.

The 2D/WBG hybrid heterostructures are expected to widen the building blocks for novel applications with unprecedented properties and excellent performance. Accordingly, it is believed that more efforts on this exciting field could open a new avenue for realizing next generation of modern electronics and optoelectronics at nanoscale.

Declaration of Competing Interest

The authors declare that they have no known competing financial interests or personal relationships that could have appeared to influence the work reported in this paper.

Acknowledgments

We gratefully acknowledge the financial support received from the National Natural Science Foundation of China (61974097, 51972279), the Fund of State Key Laboratory of Information Photonics and Optical Communications (BUPT), Sichuan Youth Science and Technology Foundation (2019JDJQ0052), and the Research Grants Council (RGC) of Hong Kong (RGC GRF No. PolyU 153023/18P), and the Fundamental Research Funds for the Central Universities.

References

[1] Novoselov KS, et al., Electric Field Effect in Atomically Thin Carbon Films, *Science*, 306 (2004) 666-669, https://doi.org/10.1126/science.1102896.
[2] Novoselov KS, VI Fal′ko, L Colombo, PR Gellert, MG Schwab, K Kim, A roadmap for graphene, *Nature*, 490 (2012) 192-200, https://doi.org/10.1038/nature11458.
[3] Wang QH, K Kalantar-Zadeh, A Kis, JN Coleman, MS Strano, Electronics and optoelectronics of two-dimensional transition metal dichalcogenides, *Nat. Nanotechnol.*, 7 (2012) 699-712, https://doi.org/10.1038/nnano.2012.193.
[4] Radisavljevic B, A Radenovic, J Brivio, V Giacometti, A Kis, Single-layer MoS_2 transistors, *Nat. Nanotechnol.*, 6 (2011) 147-150, https://doi.org/10.1038/nnano.2010.279.
[5] Mak KF, C Lee, J Hone, J Shan, TF Heinz, Atomically Thin MoS_2: A New Direct-Gap Semiconductor, *Phys. Rev. Lett.*, 105 (2010) 136805, https://doi.org/10.1103/PhysRevLett.105.136805.
[6] Li L, et al., Black phosphorus field-effect transistors, *Nat. Nanotechnol.*, 9 (2014) 372-377, https://doi.org/10.1038/nnano.2014.35.
[7] Liu H, et al., Phosphorene: An Unexplored 2D Semiconductor with a High Hole Mobility, *ACS Nano*, 8 (2014) 4033-4041, https://doi.org/10.1021/nn501226z.
[8] Eswaraiah V, Q Zeng, Y Long, Z Liu, Black Phosphorus Nanosheets: Synthesis,

Characterization and Applications, *Small*, 12 (2016) 3480-3502, https://doi.org/10.1002/smll.201600032.
[9] Mahvash F, E Paradis, D Drouin, T Szkopek, M Siaj, Space-Charge Limited Transport in Large-Area Monolayer Hexagonal Boron Nitride, *Nano Lett.*, 15 (2015) 2263-2268, https://doi.org/10.1021/nl504197c.
[10] Yen M, Y Bitla, Y-H Chu, van der Waals heteroepitaxy on muscovite, *Mater. Chem. Phys.*, 234 (2019) 185-195, https://doi.org/10.1016/j.matchemphys.2019.05.053.
[11] Novoselov KS, A Mishchenko, A Carvalho, AH Castro Neto, 2D materials and van der Waals heterostructures, *Science*, 353 (2016) aac9439, https://doi.org/10.1126/science.aac9439.
[12] Zhou X, et al., 2D Layered Material-Based van der Waals Heterostructures for Optoelectronics, *Adv. Funct. Mater.*, 28 (2018) 1706587, https://doi.org/10.1002/adfm.201706587.
[13] Dean CR, et al., Boron nitride substrates for high-quality graphene electronics, *Nat. Nanotechnol.*, 5 (2010) 722-726, https://doi.org/10.1038/nnano.2010.172.
[14] Liu Y, NO Weiss, X Duan, H-C Cheng, Y Huang, X Duan, Van der Waals heterostructures and devices, *Nat. Rev. Mater.*, 1 (2016) 16042, https://doi.org/10.1038/natrevmats.2016.42.
[15] Konstantatos G, et al., Hybrid graphene–quantum dot phototransistors with ultrahigh gain, *Nat. Nanotechnol.*, 7 (2012) 363-368, https://doi.org/10.1038/nnano.2012.60.
[16] Liao L, et al., High-speed graphene transistors with a self-aligned nanowire gate, *Nature*, 467 (2010) 305-308, https://doi.org/10.1038/nature09405.
[17] Bae S-H, et al., Integration of bulk materials with two-dimensional materials for physical coupling and applications, *Nat. Mater.*, 18 (2019) 550-560, https://doi.org/10.1038/s41563-019-0335-2.
[18] Scott JF, Applications of modern ferroelectrics, *Science*, 315 (2007) 954-959, https://doi.org/10.1126/science.1129564.
[19] Wang Y, W Jie, C Yang, X Wei, J Hao, Colossal Permittivity Materials as Superior Dielectrics for Diverse Applications, *Adv. Funct. Mater.*, 29 (2019) 1808118, https://doi.org/10.1002/adfm.201808118.
[20] Zhang Y, W Jie, P Chen, W Liu, J Hao, Ferroelectric and Piezoelectric Effects on the Optical Process in Advanced Materials and Devices, *Adv. Mater.*, 30 (2018) 1707007, https://doi.org/10.1002/adma.201707007.
[21] Fujita S, Wide-bandgap semiconductor materials: For their full bloom, *Jpn. J. Appl. Phys.*, 54 (2015) 030101, https://doi.org/10.7567/jjap.54.030101.
[22] Laturia A, ML Van de Put, WG Vandenberghe, Dielectric properties of hexagonal boron nitride and transition metal dichalcogenides: from monolayer to bulk, *npj 2D Mater. Appl.*, 2 (2018) 6, https://doi.org/10.1038/s41699-018-0050-x.
[23] Sangwan VK, MC Hersam, Electronic Transport in Two-Dimensional Materials, *Annu. Rev. Phys. Chem.*, 69 (2018) 299-325, https://doi.org/10.1146/annurev-physchem-050317-021353.
[24] Nakamura S, T Mukai, M Senoh, Candela‐class high‐brightness

InGaN/AlGaN double‐heterostructure blue‐light‐emitting diodes, *Appl. Phys. Lett.*, 64 (1994) 1687-1689, https://doi.org/10.1063/1.111832.
[25] Ozgur U, D Hofstetter, H Morkoc, ZnO Devices and Applications: A Review of Current Status and Future Prospects, *Proc. IEEE*, 98 (2010) 1255-1268, https://doi.org/10.1109/jproc.2010.2044550.
[26] Higashiwaki M, GH Jessen, Guest Editorial: The dawn of gallium oxide microelectronics, *Appl. Phys. Lett.*, 112 (2018) 060401, https://doi.org/10.1063/1.5017845.
[27] Cai Z, B Liu, X Zou, H-M Cheng, Chemical Vapor Deposition Growth and Applications of Two-Dimensional Materials and Their Heterostructures, *Chem. Rev.*, 118 (2018) 6091-6133, https://doi.org/10.1021/acs.chemrev.7b00536.
[28] Jie W, Z Yang, G Bai, J Hao, Luminescence in 2D Materials and van der Waals Heterostructures, *Adv. Opt. Mater.*, 6 (2018) 1701296, https://doi.org/10.1002/adom.201701296.
[29] Yang Z, J Hao, Recent Progress in 2D Layered III–VI Semiconductors and their Heterostructures for Optoelectronic Device Applications, *Adv. Mater. Technol.*, 4 (2019) 1900108, https://doi.org/10.1002/admt.201900108.
[30] Liu Y, Y Huang, X Duan, Van der Waals integration before and beyond two-dimensional materials, *Nature*, 567 (2019) 323-333, https://doi.org/10.1038/s41586-019-1013-x.
[31] Li T, et al., Polarization-Mediated Modulation of Electronic and Transport Properties of Hybrid MoS_2–$BaTiO_3$–$SrRuO_3$ Tunnel Junctions, *Nano Lett.*, 17 (2017) 922-927, https://doi.org/10.1021/acs.nanolett.6b04247.
[32] Xue F, et al., p-Type MoS_2 and n-Type ZnO Diode and Its Performance Enhancement by the Piezophototronic Effect, *Adv. Mater.*, 28 (2016) 3391-3398, https://doi.org/10.1002/adma.201506472.
[33] Jeon PJ, YT Lee, JY Lim, JS Kim, DK Hwang, S Im, Black Phosphorus–Zinc Oxide Nanomaterial Heterojunction for p–n Diode and Junction Field-Effect Transistor, *Nano Lett.*, 16 (2016) 1293-1298, https://doi.org/10.1021/acs.nanolett.5b04664.
[34] Kim J, MA Mastro, MJ Tadjer, J Kim, Heterostructure WSe_2−Ga_2O_3 Junction Field-Effect Transistor for Low-Dimensional High-Power Electronics, *ACS Appl. Mater. Interfaces*, 10 (2018) 29724-29729, https://doi.org/10.1021/acsami.8b07030.
[35] Xue F, et al., Enhanced photoresponsivity of the MoS_2-GaN heterojunction diode via the piezo-phototronic effect, *NPG Asia Mater.*, 9 (2017) e418-e418, https://doi.org/10.1038/am.2017.142.
[36] Yang Z, J Hao, Progress in pulsed laser deposited two-dimensional layered materials for device applications, *J. Mater. Chem. C*, 4 (2016) 8859-8878, https://doi.org/10.1039/C6TC01602B.
[37] Kong W-Y, et al., Graphene-β-Ga2O3 Heterojunction for Highly Sensitive Deep UV Photodetector Application, *Adv. Mater.*, 28 (2016) 10725-10731, https://doi.org/10.1002/adma.201604049.
[38] Ruzmetov D, et al., Vertical 2D/3D Semiconductor Heterostructures Based on Epitaxial Molybdenum Disulfide and Gallium Nitride, *ACS Nano*, 10 (2016) 3580-

3588, https://doi.org/10.1021/acsnano.5b08008.
[39] Wan Y, et al., Epitaxial Single-Layer MoS_2 on GaN with Enhanced Valley Helicity, *Adv. Mater.*, 30 (2018) 1703888, https://doi.org/10.1002/adma.201703888.
[40] Chen Z, H Liu, X Chen, G Chu, S Chu, H Zhang, Wafer-Size and Single-Crystal $MoSe_2$ Atomically Thin Films Grown on GaN Substrate for Light Emission and Harvesting, *ACS Appl. Mater. Interfaces*, 8 (2016) 20267-20273, https://doi.org/10.1021/acsami.6b04768.
[41] Zhang K, et al., Large scale 2D/3D hybrids based on gallium nitride and transition metal dichalcogenides, *Nanoscale*, 10 (2018) 336-341, https://doi.org/10.1039/C7NR07586C.
[42] Wu Z, Y Zhang, G Bai, W Tang, J Gao, J Hao, Effect of biaxial strain induced by piezoelectric PMN-PT on the upconversion photoluminescence of $BaTiO_3$:Yb/Er thin films, *Opt. Express*, 22 (2014) 29014-29019, https://doi.org/10.1364/OE.22.029014.
[43] Wu ZP, W Huang, KH Wong, JH Hao, Structural and dielectric properties of epitaxial $SrTiO_3$ films grown directly on GaAs substrates by laser molecular beam epitaxy, *J Appl Phys*, 104 (2008) 054103, https://doi.org/10.1063/1.2974796.
[44] Yang Z, et al., Field-Effect Transistors Based on Amorphous Black Phosphorus Ultrathin Films by Pulsed Laser Deposition, *Adv. Mater.*, 27 (2015) 3748-3754, https://doi.org/10.1002/adma.201500990.
[45] Yang Z, Z Wu, Y Lyu, J Hao, Centimeter-scale growth of two-dimensional layered high-mobility bismuth films by pulsed laser deposition, *InfoMat*, 1 (2019) 98-107, https://doi.org/10.1002/inf2.12001.
[46] Jiao L, et al., Layer-dependent photoresponse of 2D MoS_2 films prepared by pulsed laser deposition, *Journal of Materials Chemistry C*, 7 (2019) 2522-2529, https://doi.org/10.1039/c8tc04612c.
[47] Yang Z, et al., Wafer-Scale Synthesis of High-Quality Semiconducting Two-Dimensional Layered InSe with Broadband Photoresponse, *ACS Nano*, 11 (2017) 4225-4236, https://doi.org/10.1021/acsnano.7b01168.
[48] Serna MI, et al., Large-Area Deposition of MoS_2 by Pulsed Laser Deposition with In Situ Thickness Control, *ACS Nano*, 10 (2016) 6054-6061, https://doi.org/10.1021/acsnano.6b01636.
[49] Serrao CR, et al., Highly crystalline MoS_2 thin films grown by pulsed laser deposition, *Appl. Phys. Lett.*, 106 (2015) 052101, https://doi.org/10.1063/1.4907169.
[50] Chromik Š, M Sojková, V Vretenár, A Rosová, E Dobročka, M Hulman, Influence of GaN/AlGaN/GaN (0001) and Si (100) substrates on structural properties of extremely thin MoS_2 films grown by pulsed laser deposition, *Appl. Surf. Sci.*, 395 (2017) 232-236, https://doi.org/https://doi.org/10.1016/j.apsusc.2016.06.038.
[51] Ho Y-T, et al., Layered MoS_2 grown on c -sapphire by pulsed laser deposition, *Phys. Status Solidi RRL*, 9 (2015) 187-191, https://doi.org/10.1002/pssr.201409561.
[52] Liao W, Y Huang, H Wang, H Zhang, Van der Waals heterostructures for optoelectronics: Progress and prospects, *Appl. Mater. Today*, 16 (2019) 435-455, https://doi.org/10.1016/j.apmt.2019.07.004.
[53] Schwartz JJ, et al., Chemical Identification of Interlayer Contaminants within van der Waals Heterostructures, *ACS Appl. Mater. Interfaces*, 11 (2019) 25578-25585,

https://doi.org/10.1021/acsami.9b06594.
[54] Xin H, Q Zhao, D Chen, W Li, Roll-to-Roll Mechanical Peeling for Dry Transfer of Chemical Vapor Deposition Graphene, *J. Micro Nano-Manuf.*, 6 (2018), https://doi.org/10.1115/1.4040449.
[55] Kroemer H, Nobel Lecture: Quasielectric fields and band offsets: teaching electrons new tricks, *Rev. Mod. Phys.*, 73 (2001) 783-793, https://doi.org/10.1103/RevModPhys.73.783.
[56] Anderson R, Germanium-gallium arsenide heterojunctions, *IBM J. Res. Dev.*, 4 (1960) 283-287, https://doi.org/10.1147/rd.43.0283.
[57] Tersoff J, Theory of semiconductor heterojunctions: The role of quantum dipoles, *Phys. Rev. B*, 30 (1984) 4874, https://doi.org/10.1103/PhysRevB.30.4874.
[58] Sze SM, KK Ng, Physics of semiconductor devices, John wiley & sons 2006.
[59] Tung RT, The physics and chemistry of the Schottky barrier height, *Appl. Phys. Rev.*, 1 (2014) 011304, https://doi.org/10.1063/1.4858400.
[60] Liu Y, et al., Approaching the Schottky–Mott limit in van der Waals metal–semiconductor junctions, *Nature*, 557 (2018) 696-700, https://doi.org/10.1038/s41586-018-0129-8.
[61] Zhang Z, Q Qian, B Li, KJ Chen, Interface Engineering of Monolayer MoS_2/GaN Hybrid Heterostructure: Modified Band Alignment for Photocatalytic Water Splitting Application by Nitridation Treatment, *ACS Appl Mater Interfaces*, 10 (2018) 17419-17426, https://doi.org/10.1021/acsami.8b01286.
[62] Oostinga JB, HB Heersche, X Liu, AF Morpurgo, LM Vandersypen, Gate-induced insulating state in bilayer graphene devices, *Nat. Mater.*, 7 (2008) 151-157, https://doi.org/10.1038/nmat2082.
[63] MacNeill D, G Stiehl, M Guimaraes, R Buhrman, J Park, D Ralph, Control of spin–orbit torques through crystal symmetry in WTe_2/ferromagnet bilayers, *Nat. Phys.*, 13 (2017) 300-305, https://doi.org/10.1038/nphys3933.
[64] Tang S, et al., Quantum spin Hall state in monolayer 1T'-WTe 2, *Nat. Phys.*, 13 (2017) 683-687, https://doi.org/10.1038/nphys4174.
[65] Fei Z, et al., Edge conduction in monolayer WTe_2, *Nat. Phys.*, 13 (2017) 677-682, https://doi.org/10.1038/nphys4091.
[66] Qi Y, et al., Superconductivity in Weyl semimetal candidate $MoTe_2$, *Nat. Commun.*, 7 (2016) 1-7, https://doi.org/10.1038/ncomms11038.
[67] Cho S, et al., Phase patterning for ohmic homojunction contact in $MoTe_2$, *Science*, 349 (2015) 625-628, https://doi.org/10.1126/science.aab3175.
[68] Li L, et al., Black phosphorus field-effect transistors, *Nat Nanotechnol*, 9 (2014) 372-377, https://doi.org/10.1038/nnano.2014.35.
[69] Yang J, et al., Optical tuning of exciton and trion emissions in monolayer phosphorene, *Light-Sci. Appl.*, 4 (2015) e312-e312, https://doi.org/10.1038/lsa.2015.85.
[70] Liu H, Y Du, Y Deng, PD Ye, Semiconducting black phosphorus: synthesis, transport properties and electronic applications, *Chem. Soc. Rev.*, 44 (2015) 2732-2743, https://doi.org/10.1039/c4cs00257a.
[71] Yang Z, J Hao, Recent Progress in Black-Phosphorus-Based Heterostructures for

Device Applications, *Small Methods*, 2 (2018) 1700296, https://doi.org/10.1002/smtd.201700296.
[72] Bandurin DA, et al., High electron mobility, quantum Hall effect and anomalous optical response in atomically thin InSe, *Nat. Nanotechnol.*, 12 (2017) 223-227, https://doi.org/10.1038/nnano.2016.242.
[73] Yang Z, et al., Wafer-Scale Synthesis of High-Quality Semiconducting Two-Dimensional Layered InSe with Broadband Photoresponse, *ACS Nano*, 11 (2017) 4225-4236, https://doi.org/10.1021/acsnano.7b01168.
[74] Mudd GW, et al., Tuning the bandgap of exfoliated InSe nanosheets by quantum confinement, *Adv. Mater.*, 25 (2013) 5714-5718, https://doi.org/10.1002/adma.201302616.
[75] van der Zande AM, et al., Grains and grain boundaries in highly crystalline monolayer molybdenum disulphide, *Nat. Mater.*, 12 (2013) 554-561, https://doi.org/10.1038/nmat3633.
[76] Splendiani A, et al., Emerging photoluminescence in monolayer MoS_2, *Nano Lett.*, 10 (2010) 1271-1275, https://doi.org/10.1021/nl903868w.
[77] Zhou H, et al., Large area growth and electrical properties of p-type WSe_2 atomic layers, *Nano Lett.*, 15 (2015) 709-713, https://doi.org/10.1021/nl504256y.
[78] Desai SB, et al., Strain-induced indirect to direct bandgap transition in multilayer WSe_2, *Nano Lett.*, 14 (2014) 4592-4597, https://doi.org/10.1021/nl501638a.
[79] Topsakal M, E Akturk, S Ciraci, First-principles study of two- and one-dimensional honeycomb structures of boron nitride, *Phys. Rev. B*, 79 (2009) 115442, https://doi.org/10.1103/PhysRevB.79.115442.
[80] Nakamura S, M Senoh, N Iwasa, S-i Nagahama, High-brightness InGaN blue, green and yellow light-emitting diodes with quantum well structures, *Jpn. J. Appl. Phys.*, 34 (1995) L797, https://doi.org/10.1143/JJAP.34.L797.
[81] Arakawa Y, A Yariv, Quantum well lasers-Gain, spectra, dynamics, *IEEE J. Quantum Electron.*, 22 (1986) 1887-1899, https://doi.org/10.1109/JQE.1986.1073185.
[82] Withers F, et al., Light-emitting diodes by band-structure engineering in van der Waals heterostructures, *Nat. Mater.*, 14 (2015) 301-306, https://doi.org/10.1038/nmat4205.
[83] Lin YD, et al., High Quality InGaN/AlGaN Multiple Quantum Wells for Semipolar InGaN Green Laser Diodes, *Appl. Phys. Express*, 3 (2010) 082001, https://doi.org/10.1143/Apex.3.082001.
[84] Zhang H, Y-N Zhang, H Liu, L-M Liu, Novel heterostructures by stacking layered molybdenum disulfides and nitrides for solar energy conversion, *J. Mater. Chem. A*, 2 (2014) 15389-15395, https://doi.org/10.1039/C4TA03134B.
[85] Koswatta SO, SJ Koester, W Haensch, On the Possibility of Obtaining MOSFET-Like Performance and Sub-60-mV/dec Swing in 1-D Broken-Gap Tunnel Transistors, *IEEE Trans. Electron Devices*, 57 (2010) 3222-3230, https://doi.org/10.1109/Ted.2010.2079250.
[86] Rao Y-C, S Yu, X-M Duan, Electrical and optical behaviors of SiC(GeC)/MoS_2 heterostructures: a first principles study, *Phys. Chem. Chem. Phys.*, 19 (2017) 17250-17255, https://doi.org/10.1039/C7CP02616A.

[87] Liao J, B Sa, J Zhou, R Ahuja, Z Sun, Design of High-Efficiency Visible-Light Photocatalysts for Water Splitting: MoS_2/AlN(GaN) Heterostructures, *J. Phys. Chem. C*, 118 (2014) 17594-17599, https://doi.org/10.1021/jp5038014.
[88] Ozcelik VO, JG Azadani, C Yang, SJ Koester, T Low, Band alignment of two-dimensional semiconductors for designing heterostructures with momentum space matching, *Phys. Rev. B*, 94 (2016) 035125, https://doi.org/10.1103/PhysRevB.94.035125.
[89] Ouyang B, P Ou, Y Wang, Z Mi, J Song, Phase engineering of MoS_2 through GaN/AlN substrate coupling and electron doping, *Phys. Chem. Chem. Phys.*, 18 (2016) 33351-33356, https://doi.org/10.1039/C6CP05404H.
[90] Fang Q, et al., Interfacial electronic states and self-formed p–n junctions in hydrogenated MoS_2/SiC heterostructure, *J. Mater. Chem. C*, 6 (2018) 4523-4530, https://doi.org/10.1039/C8TC00742J.
[91] Haratipour N, MC Robbins, SJ Koester, Black phosphorus p-MOSFETs with 7-nm HfO_2 gate dielectric and low contact resistance, *IEEE Electron Device Lett.*, 36 (2015) 411-413, https://doi.org/10.1109/LED.2015.2407195.
[92] Chhowalla M, D Jena, H Zhang, Two-dimensional semiconductors for transistors, *Nat. Rev. Mater.*, 1 (2016) 1-15, https://doi.org/10.1038/natrevmats2016.52.
[93] Kraut EA, RW Grant, JR Waldrop, SP Kowalczyk, Precise Determination of the Valence-Band Edge in X-Ray Photoemission Spectra: Application to Measurement of Semiconductor Interface Potentials, *Phys. Rev. Lett.*, 44 (1980) 1620-1623, https://doi.org/10.1103/PhysRevLett.44.1620.
[94] Jie W, J Hao, Graphene-based hybrid structures combined with functional materials of ferroelectrics and semiconductors, *Nanoscale*, 6 (2014) 6346-6362, https://doi.org/10.1039/C3NR06918D.
[95] Hong X, A Posadas, K Zou, CH Ahn, J Zhu, High-mobility few-layer graphene field effect transistors fabricated on epitaxial ferroelectric gate oxides, *Phys. Rev. Lett.*, 102 (2009) 136808, https://doi.org/10.1103/PhysRevLett.102.136808.
[96] Zheng Y, et al., Wafer-scale graphene/ferroelectric hybrid devices for low-voltage electronics, *EPL*, 93 (2011) 17002, https://doi.org/10.1209/0295-5075/93/17002.
[97] Zheng Y, et al., Gate-controlled nonvolatile graphene-ferroelectric memory, *Appl. Phys. Lett.*, 94 (2009) 163505, https://doi.org/10.1063/1.3119215.
[98] Zheng Y, G-X Ni, C-T Toh, C-Y Tan, K Yao, B Özyilmaz, Graphene Field-Effect Transistors with Ferroelectric Gating, *Phys. Rev. Lett.*, 105 (2010) 166602, https://doi.org/10.1103/PhysRevLett.105.166602.
[99] Jie W, YY Hui, NY Chan, Y Zhang, SP Lau, J Hao, Ferroelectric Polarization Effects on the Transport Properties of Graphene/PMN-PT Field Effect Transistors, *J. Phys. Chem. C*, 117 (2013) 13747-13752, https://doi.org/10.1021/jp404350r.
[100] Jie W, J Hao, Time-dependent transport characteristics of graphene tuned by ferroelectric polarization and interface charge trapping, *Nanoscale*, 10 (2018) 328-335, https://doi.org/10.1039/C7NR06485C.
[101] Lipatov A, P Sharma, A Gruverman, A Sinitskii, Optoelectrical Molybdenum Disulfide (MoS_2)—Ferroelectric Memories, *ACS Nano*, 9 (2015) 8089-8098,

https://doi.org/10.1021/acsnano.5b02078.
[102] Ko C, et al., Ferroelectrically Gated Atomically Thin Transition-Metal Dichalcogenides as Nonvolatile Memory, *Adv. Mater.*, 28 (2016) 2923-2930, https://doi.org/10.1002/adma.201504779.
[103] Wang X, et al., Ultrasensitive and Broadband MoS2 Photodetector Driven by Ferroelectrics, *Adv. Mater.*, 27 (2015) 6575-6581, https://doi.org/10.1002/adma.201503340.
[104] Nguyen A, et al., Toward Ferroelectric Control of Monolayer MoS_2, *Nano Lett.*, 15 (2015) 3364-3369, https://doi.org/10.1021/acs.nanolett.5b00687.
[105] Baeumer C, SP Rogers, R Xu, LW Martin, M Shim, Tunable Carrier Type and Density in Graphene/$PbZr_{0.2}Ti_{0.8}O_3$ Hybrid Structures through Ferroelectric Switching, *Nano Lett.*, 13 (2013) 1693-1698, https://doi.org/10.1021/nl4002052.
[106] Yuan S, et al., Ferroelectric-Driven Performance Enhancement of Graphene Field-Effect Transistors Based on Vertical Tunneling Heterostructures, *Adv. Mater.*, 28 (2016) 10048-10054, https://doi.org/10.1002/adma.201601489.
[107] Jie W, YY Hui, Y Zhang, SP Lau, J Hao, Effects of controllable biaxial strain on the Raman spectra of monolayer graphene prepared by chemical vapor deposition, *Appl. Phys. Lett.*, 102 (2013) 223112, https://doi.org/10.1063/1.4809922.
[108] Hao J, C-N Xu, Piezophotonics: From fundamentals and materials to applications, *MRS Bulletin*, 43 (2018) 965-969, https://doi.org/10.1557/mrs.2018.296.
[109] Hui YY, et al., Exceptional tunability of band energy in a compressively strained trilayer MoS_2 sheet, *ACS Nano*, 7 (2013) 7126-7131, https://doi.org/10.1021/nn4024834.
[110] Conley HJ, B Wang, JI Ziegler, RF Haglund, ST Pantelides, KI Bolotin, Bandgap Engineering of Strained Monolayer and Bilayer MoS2, *Nano Lett.*, 13 (2013) 3626-3630, https://doi.org/10.1021/nl4014748.
[111] Wang Y, et al., Strain-induced direct–indirect bandgap transition and phonon modulation in monolayer WS_2, *Nano Res.*, 8 (2015) 2562-2572, https://doi.org/10.1007/s12274-015-0762-6.
[112] Iff O, et al., Strain-Tunable Single Photon Sources in WSe_2 Monolayers, *Nano Lett.*, 19 (2019) 6931-6936, https://doi.org/10.1021/acs.nanolett.9b02221.
[113] Nie B, et al., Monolayer Graphene Film on ZnO Nanorod Array for High-Performance Schottky Junction Ultraviolet Photodetectors, *Small*, 9 (2013) 2872-2879, https://doi.org/10.1002/smll.201203188.
[114] Lin F, et al., Graphene/GaN diodes for ultraviolet and visible photodetectors, *Appl. Phys. Lett.*, 105 (2014) 073103, https://doi.org/10.1063/1.4893609.
[115] Journot T, V Bouchiat, B Gayral, J Dijon, B Hyot, Self-Assembled UV Photodetector Made by Direct Epitaxial GaN Growth on Graphene, *ACS Appl. Mater. Interfaces*, 10 (2018) 18857-18862, https://doi.org/10.1021/acsami.8b01194.
[116] Anderson TJ, et al., Ultraviolet detector based on graphene/SiC heterojunction, *Appl. Phys. Express*, 8 (2015) 041301, https://doi.org/10.7567/apex.8.041301.
[117] Ai ML, et al., Fast-response solar-blind ultraviolet photodetector with a graphene/beta-Ga_2O_3/graphene hybrid structure, *J Alloy Compd*, 692 (2017) 634-638, https://doi.org/10.1016/j.jallcom.2016.09.087.

[118] Kim S, S Oh, J Kim, Ultrahigh Deep-UV Sensitivity in Graphene-Gated β-Ga_2O_3 Phototransistors, *ACS Photonics*, 6 (2019) 1026-1032, https://doi.org/10.1021/acsphotonics.9b00032.
[119] Wei M, K Yao, Y Liu, C Yang, X Zang, L Lin, A Solar-Blind UV Detector Based on Graphene-Microcrystalline Diamond Heterojunctions, *Small*, 13 (2017) 1701328, https://doi.org/10.1002/smll.201701328.
[120] Zhuo R, et al., High-performance self-powered deep ultraviolet photodetector based on MoS_2/GaN p–n heterojunction, *J. Mater. Chem. C*, 6 (2018) 299-303, https://doi.org/10.1039/C7TC04754A.
[121] Zhao Z, et al., Synthesis of large-area 2D WS_2 films and fabrication of a heterostructure for self-powered ultraviolet photodetection and imaging applications, *J. Mater. Chem. C*, 7 (2019) 12121-12126, https://doi.org/10.1039/C9TC03866C.
[122] Zhuo R, et al., A self-powered solar-blind photodetector based on a MoS_2/β-Ga_2O_3 heterojunction, *J. Mater. Chem. C*, 6 (2018) 10982-10986, https://doi.org/10.1039/C8TC04258F.
[123] Yang H, et al., Graphene Barristor, a Triode Device with a Gate-Controlled Schottky Barrier, *Science*, 336 (2012) 1140-1143, https://doi.org/10.1126/science.1220527.
[124] Hwang HJ, et al., A graphene barristor using nitrogen profile controlled ZnO Schottky contacts, *Nanoscale*, 9 (2017) 2442-2448, https://doi.org/10.1039/C6NR08829E.
[125] Kumar A, R Kashid, A Ghosh, V Kumar, R Singh, Enhanced Thermionic Emission and Low 1/f Noise in Exfoliated Graphene/GaN Schottky Barrier Diode, *ACS Appl. Mater. Interfaces*, 8 (2016) 8213-8223, https://doi.org/10.1021/acsami.5b12393.
[126] Yan X, IS Esqueda, J Ma, J Tice, H Wang, High breakdown electric field in β-Ga_2O_3/graphene vertical barristor heterostructure, *Appl. Phys. Lett.*, 112 (2018) 032101, https://doi.org/10.1063/1.5002138.
[127] Kim J, J Kim, Monolithically Integrated Enhancement-Mode and Depletion-Mode beta-Ga_2O_3 MESFETs with Graphene-Gate Architectures and Their Logic Applications, *ACS Appl. Mater. Interfaces*, 12 (2020) 7310-7316, https://doi.org/10.1021/acsami.9b19667.
[128] Yan Z, G Liu, JM Khan, AA Balandin, Graphene quilts for thermal management of high-power GaN transistors, *Nat. Commun.*, 3 (2012) 827, https://doi.org/10.1038/ncomms1828.
[129] Kim J, MA Mastro, MJ Tadjer, J Kim, Quasi-Two-Dimensional h-BN/β-Ga_2O_3 Heterostructure Metal–Insulator–Semiconductor Field-Effect Transistor, *ACS Appl. Mater. Interfaces*, 9 (2017) 21322-21327, https://doi.org/10.1021/acsami.7b04374.
[130] Kudo A, Y Miseki, Heterogeneous photocatalyst materials for water splitting, *Chem. Soc. Rev.*, 38 (2009) 253-278, https://doi.org/10.1039/B800489G.
[131] Qu Y, X Duan, Progress, challenge and perspective of heterogeneous photocatalysts, *Chem. Soc. Rev.*, 42 (2013) 2568-2580, https://doi.org/10.1039/C2CS35355E.
[132] Yang Q, et al., AlN/BP heterostructure photocatalyst for water splitting, *IEEE*

Electron Device Lett., 38 (2016) 145-148, https://doi.org/10.1109/LED.2016.2633487.
[133] Selvaraj R, KR Kalimuthu, V Kalimuthu, A type-II MoS_2/ZnO heterostructure with enhanced photocatalytic activity, *Mater. Lett.*, 243 (2019) 183-186, https://doi.org/https://doi.org/10.1016/j.matlet.2019.02.022.
[134] Yang Q, et al., Considering the spin–orbit coupling effect on the photocatalytic performance of AlN/MX_2 nanocomposites, *J. Mater. Chem. C*, 5 (2017) 9412-9420, https://doi.org/10.1039/C7TC02461D.
[135] Fang Q, Y Huang, Y Miao, K Xu, Y Li, F Ma, Interfacial Defect Engineering on Electronic States of Two-Dimensional AlN/MoS_2 Heterostructure, *J. Phys. Chem. C*, 121 (2017) 6605-6613, https://doi.org/10.1021/acs.jpcc.6b11270.
[136] Zhang Z, Q Qian, B Li, KJ Chen, Interface Engineering of Monolayer MoS2/GaN Hybrid Heterostructure: Modified Band Alignment for Photocatalytic Water Splitting Application by Nitridation Treatment, *ACS Appl. Mater. Interfaces*, 10 (2018) 17419-17426, https://doi.org/10.1021/acsami.8b01286.
[137] Chen Y, et al., Unusual Mechanism Behind Enhanced Photocatalytic Activity and Surface Passivation of SiC(0001) via Forming Heterostructure with a MoS_2 Monolayer, *J. Phys. Chem. C*, 124 (2020) 1362-1368, https://doi.org/10.1021/acs.jpcc.9b08740.
[138] Meng Z, RM Stolz, L Mendecki, KA Mirica, Electrically-transduced chemical sensors based on two-dimensional nanomaterials, *Chem. Rev.*, 119 (2019) 478-598, https://doi.org/10.1021/acs.chemrev.8b00311.
[139] Yuan W, G Shi, Graphene-based gas sensors, *J. Mater. Chem. A*, 1 (2013) 10078-10091, https://doi.org/10.1039/C3TA11774J.
[140] Mao S, et al., Two-dimensional nanomaterial-based field-effect transistors for chemical and biological sensing, *Chem. Soc. Rev.*, 46 (2017) 6872-6904, https://doi.org/10.1039/C6CS00827E.
[141] Wu Z, et al., Nanowire-Seeded Growth of Single-Crystalline (010)-Ga_2O_3 Nanosheets with High Field-Effect Electron Mobility and On/Off Current Ratio, *Small*, 15 (2019), https://doi.org/10.1002/smll.201900580.
[142] Bag A, N-E Lee, Gas sensing with heterostructures based on two-dimensional nanostructured materials: a review, *J. Mater. Chem. C*, 7 (2019) 13367-13383, https://doi.org/10.1039/C9TC04132J.
[143] Yuan X, et al., Direct Synthesis of Upstanding Graphene/ZnO Nanowalls/Graphene Sandwich Heterojunction and Its Application for NO_2 Gas Sensor, *J. Nanosci. Nanotechnol.*, 19 (2019) 7947-7952, https://doi.org/10.1166/jnn.2019.16856.
[144] Han Y, et al., Design of Hetero-Nanostructures on MoS_2 Nanosheets To Boost NO_2 Room-Temperature Sensing, *ACS Appl. Mater. Interfaces*, 10 (2018) 22640-22649, https://doi.org/10.1021/acsami.8b05811.
[145] Reddeppa M, et al., H2, H2S gas sensing properties of rGO/GaN nanorods at room temperature: Effect of UV illumination, *Sensor Actuat. B-Chem*, 264 (2018) 353-362, https://doi.org/10.1016/j.snb.2018.03.018.
[146] Reddeppa M, et al., Solution-processed Au@rGO/GaN nanorods hybrid-structure for self-powered UV, visible photodetector and CO gas sensors, *Curr. Appl.*

Phys., 19 (2019) 938-945, https://doi.org/10.1016/j.cap.2019.05.008.
[147] Goel N, et al., A high-performance hydrogen sensor based on a reverse-biased MoS_2/GaN heterojunction, *Nanotechnology*, 30 (2019), https://doi.org/10.1088/1361-6528/ab1102.
[148] Minh Triet N, et al., High-Performance Schottky Diode Gas Sensor Based on the Heterojunction of Three-Dimensional Nanohybrids of Reduced Graphene Oxide – Vertical ZnO Nanorods on an AlGaN/GaN Layer, *ACS Appl. Mater. Interfaces*, 9 (2017) 30722-30732, https://doi.org/10.1021/acsami.7b06461.
[149] Bag A, D-B Moon, K-H Park, C-Y Cho, N-E Lee, Room-temperature-operated fast and reversible vertical-heterostructure-diode gas sensor composed of reduced graphene oxide and AlGaN/GaN, *Sensor Actuat. B-Chem*, 296 (2019) 126684, https://doi.org/10.1016/j.snb.2019.126684.

Table I. Basic physical properties of selected monolayer 2D materials and single-crystal wide-bandgap semiconductors, including: bandgap, dielectric constant, breakdown electric field, electron mobility and thermal conductivity. Sources are taken from ref. [21-23].

	2D materials					WBG semiconductors				
	Graphene	MoS_2	WSe_2	BP	h-BN	ZnO	SiC	GaN	Ga_2O_3	diamond
Bandgap (eV)	-	1.89	1.6	2	6	3.35	3.2	3.4	4.9	5.5
Dielectric constant	-	15.3	15.3	-	6.82	8.7	10	9	10	5.7
Breakdown field (MV/cm)	-	-	-	-	12		2.5	3.3	8	20
Electron mobility (cm^2/Vs)	15000	480	142	1000	-	200	1000	1250	300	4500
Thermal conductivity (W/cmK)	35	0.34	0.04	1.52	7.51	0.6	4.9	2.3	0.23	24

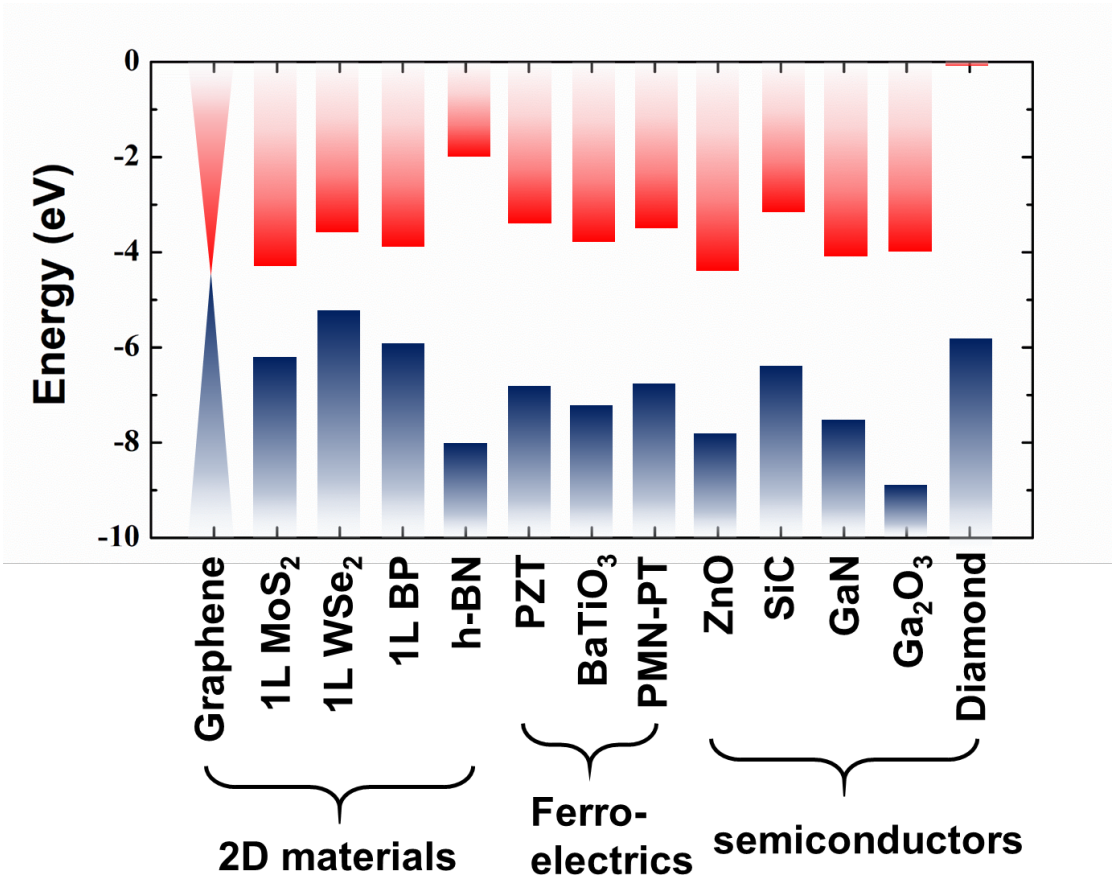

Fig. 1. Schematic band diagram of common 2D materials, wide bandgap semiconductors and ferroelectrics according to the bandgaps and electron affinities from literatures.

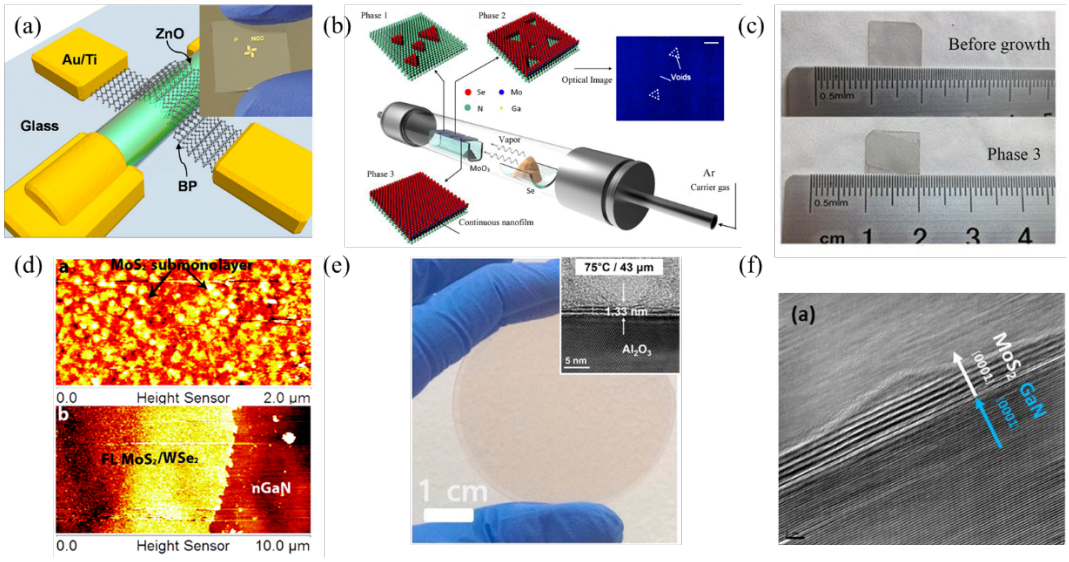

Fig. 2. (a) The schematic image of BP-ZnO heterojunction. The inset shows the corresponding optical image [33]. (b) The schematic of fabrication process of $MoSe_2$ by CVD. Three sectional phases are highlighted in the left side of the image. The inset of right side shows the optical image of phase 2. Scale bar: 10 μm. (c) Photograph of bare GaN substrate and $MoSe_2$ film of phase 3 [40]. (d) AFM images of monolayer MoS_2/monolayer WSe_2/GaN (up) and few-layer MoS_2/few-layer WSe_2/GaN (down), respectively [41]. (e) Optical image of wafer-scale MoS_2 grown on sapphire substrate. The inset shows the cross-sectional TEM image of MoS_2 nanosheet [48]. (f) Cross-sectional TEM image of MoS_2/GaN (0001). Scale bar: 1 nm [49].

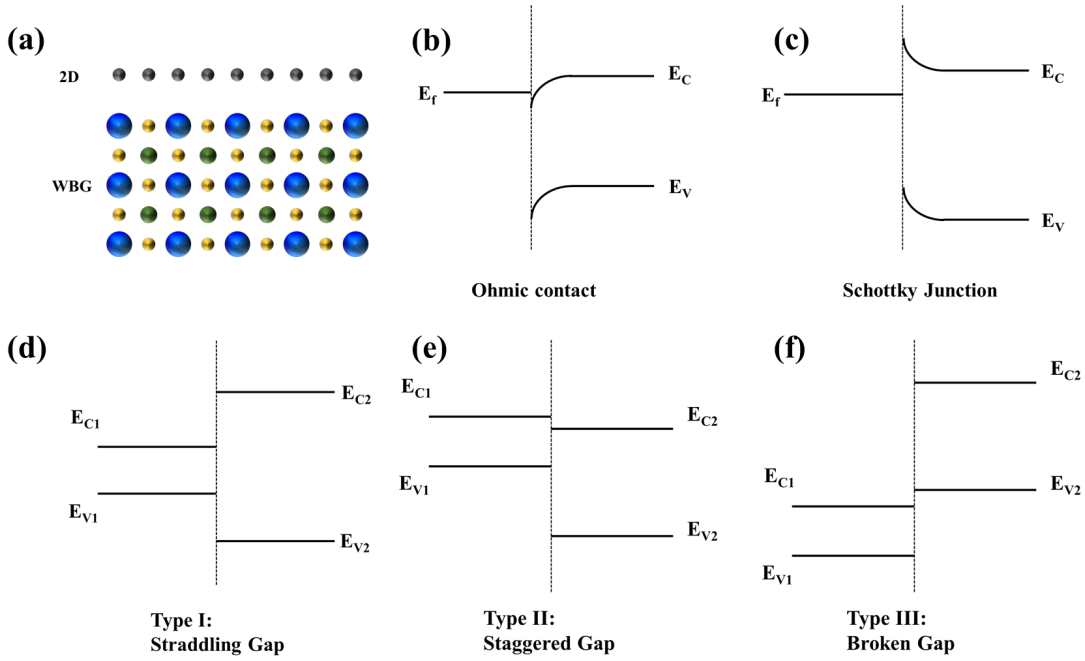

Fig. 3. (a) Schematic atomic structure and various band alignments of 2D/WBG vdW heterostructures: (b) Ohmic contact, (c) Schottky junction, (d) Type I Straddling gap, (e) Type II Staggered gap, and (f) Type III Broken gap.

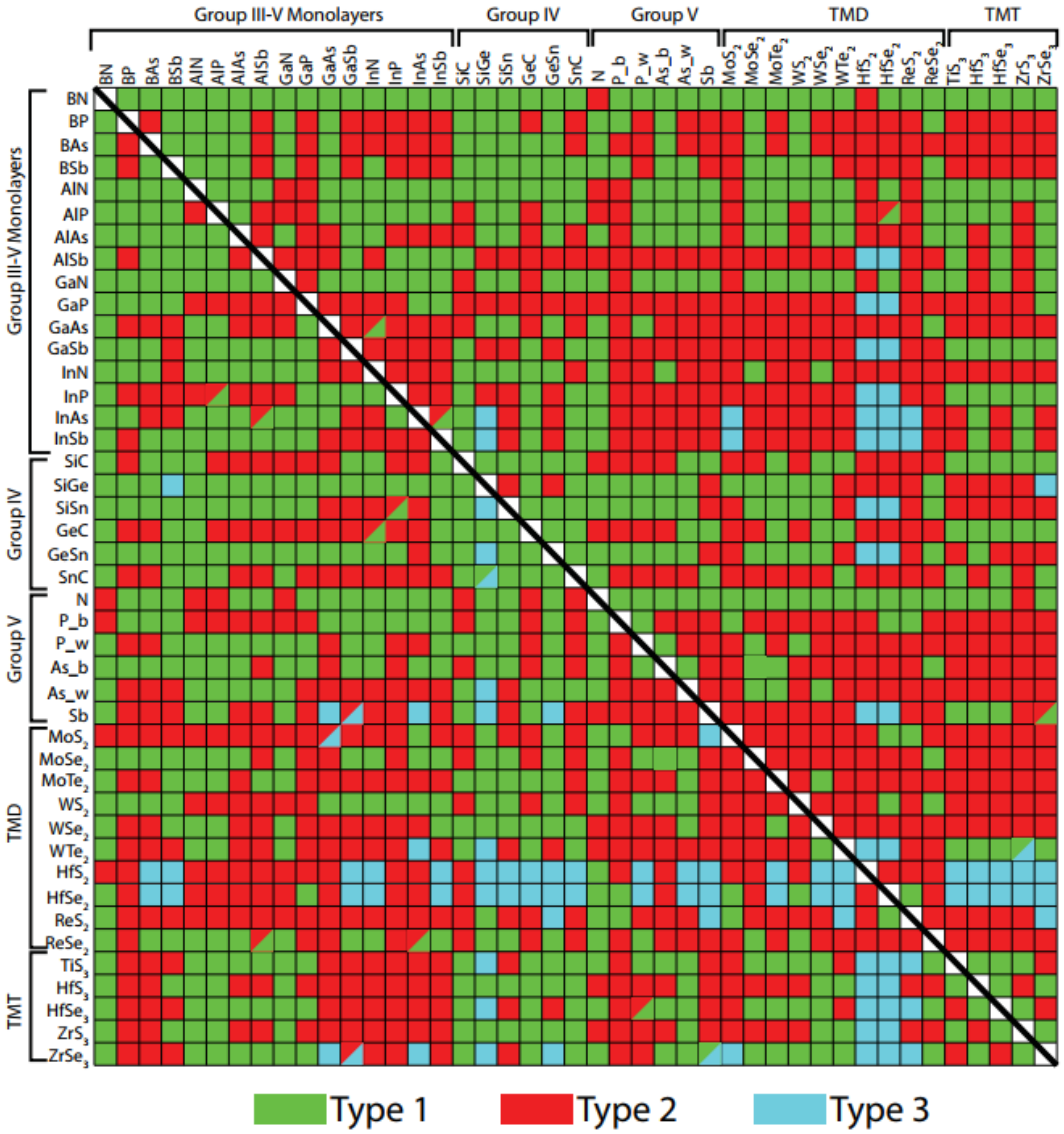

Fig. 4. Periodic table of vdW heterostructures band alignments calculated using PBE (lower left region) and HSE06 (top right region). Green, red, and blue denote Type I, II, and III heterostructure type, respectively. Two-colored boxes indicate equal chances of two different types, owing to the same formation energy within the error range of the DFT calculation [88].

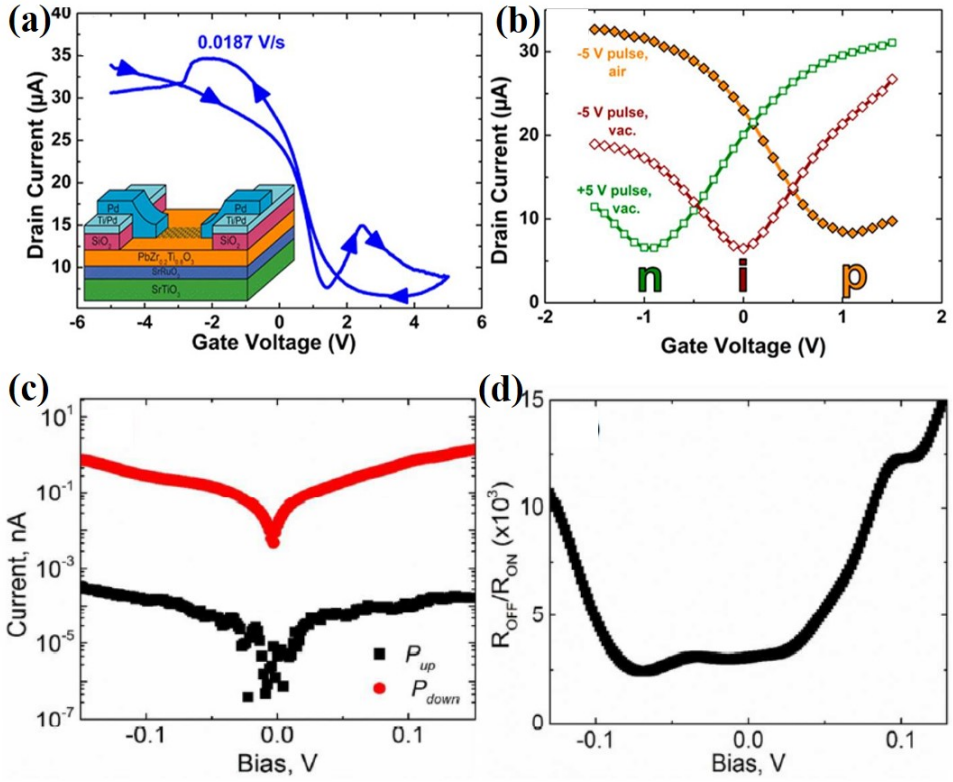

Fig. 5. Heterostructures based on 2D materials and ferroelectrics. (a) The transport properties of graphene. Inset shows the schematics of graphene/PZT heterostructure [105]. (b) The transport properties of graphene tuned by the additional initial pulse voltages in air and in vacuum. (c) The *I*−*V* characteristics of the FTJ based on MoS_2 and BTO [31]. (d) The resistance OFF/ON ratio as a function of the bias voltage.

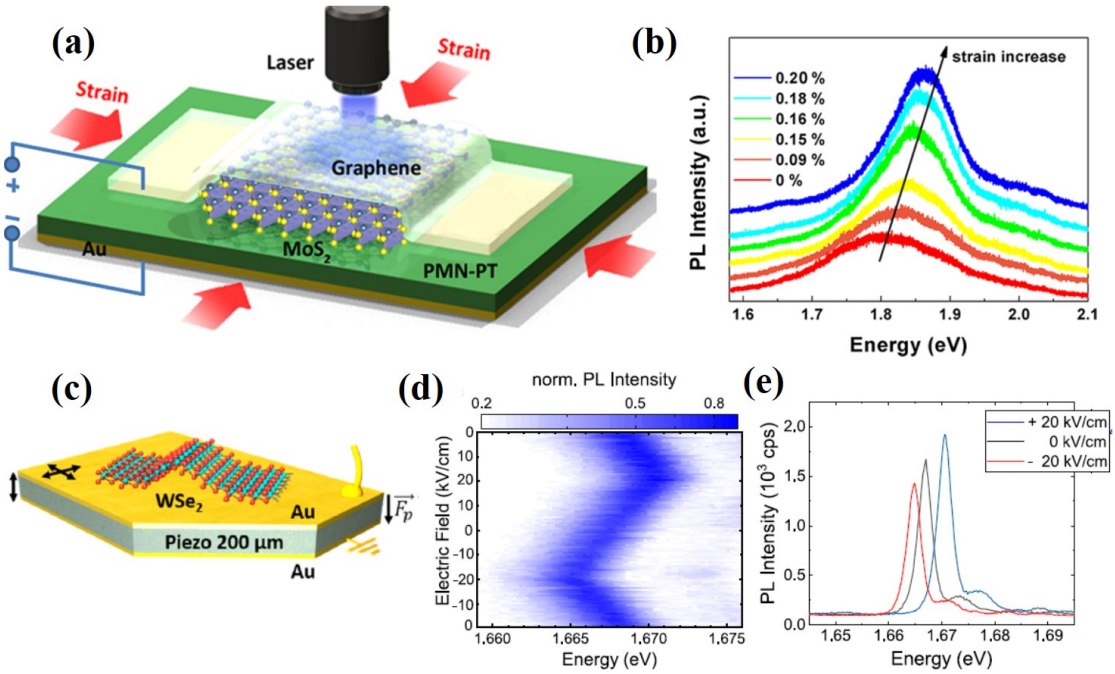

Fig. 6. Heterostructures based on 2D materials and piezoelectric PMN-PT. (a) Schematics of graphene/MoS_2/PMN-PT heterostructure [109]. (b) The PL spectra of MoS_2 tuned by the piezoelectric biaxial strain from 0 to 0.2%. (c) Schematics of WSe_2/PMN-PT heterostructure [112]. (d) The micro-PL spectra of a SPE tuned by the applied electric field from −20 to 20 kV/cm on the PMN-PT. (e) The micro-PL spectra of the SPE tuned by the electric fields of −20 and 20 kV/cm on the PMN-PT (red and blue lines).

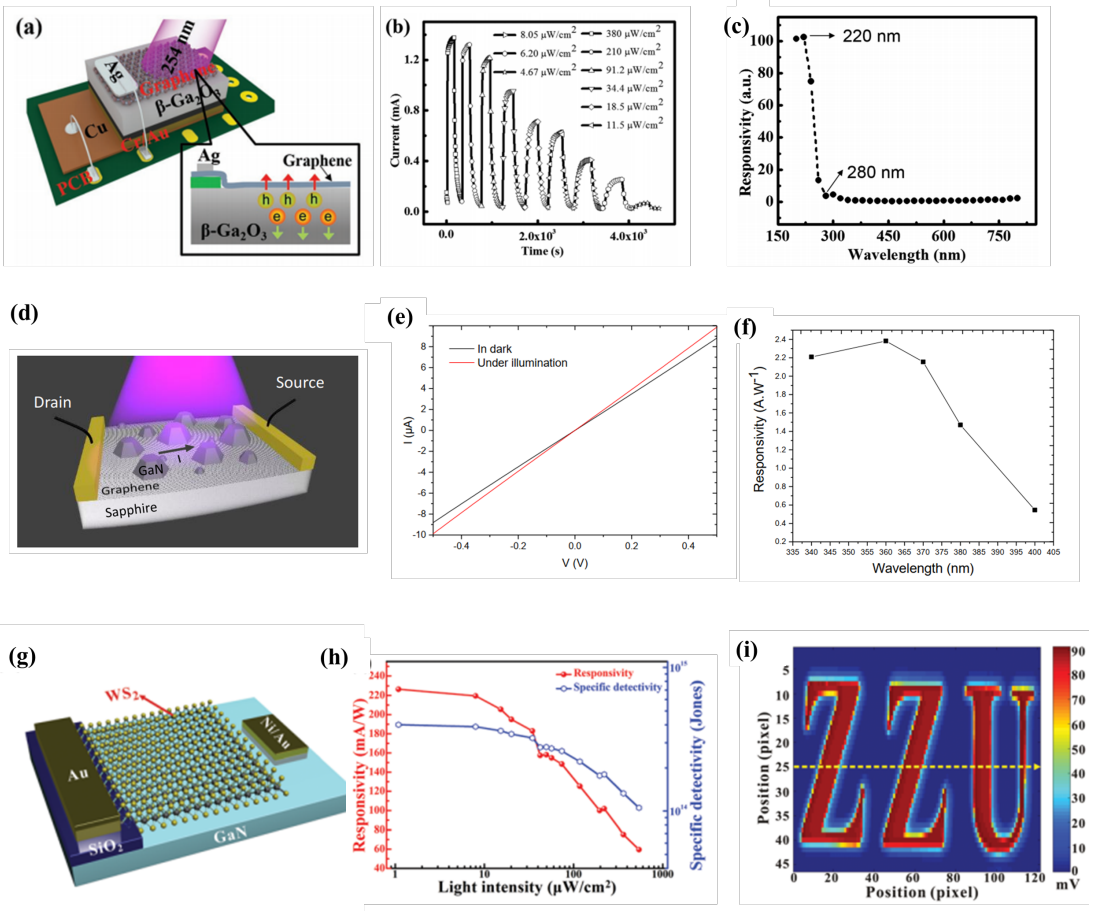

Fig. 7. Photodetectors. (a) Schematic diagram of graphene/Ga_2O_3 Schottky junction photodetector [37]. (b) Photoresponse of the device in (a) under different light intensities. (c) spectral selectivity of the device in (a). (d) Schematic diagram of self-assembled GaN/graphene photodetector [115]. (e) Current-Voltage curves measured with and without 360 nm light illumination. (f) Spectral response of the device in (d). (g) Schematic diagram of the WS_2/GaN photodetector [121]. (h) Responsivity and specific detectivity of the device in (g) as a function of light intensity. (i) The UV imaging results using device in (g).

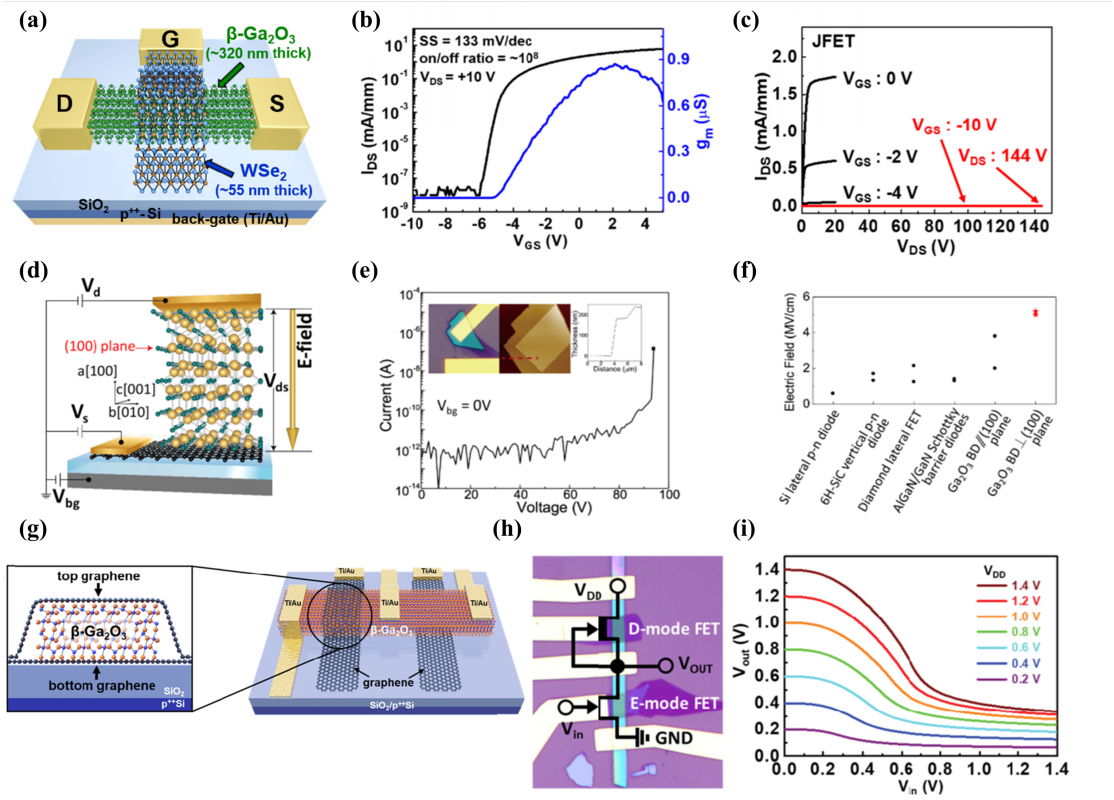

Fig. 8. Field effect transistors. (a) Schematic diagram of Ga_2O_3/WSe_2 Junction Field effect transistor, a SiO_2 (300 nm)/p^{++}−Si (500 μm) substrate was used as the back-gate. (b) Transfer and transconductance characteristics of the device in (a). (c) Three-terminal breakdown measurement of the device in (a), a breakdown voltage of 144 V is obtained at V_{GS} = -10 V [34]. (d) Schematic diagram of a vertical Ga_2O_3/graphene barristor device. (e) The off-state breakdown voltage of the barristor device shown in (d). (f) Comparisons of breakdown electric fields of the device in (d) with other reported power devices [126]. (g) Schematic diagram of the integrated E-/D-mode graphene/Ga_2O_3 MESFETs. (h) Direct coupled FET logic inverter based on device shown in (g). (i) The voltage transfer characteristics of the logic inverter presented in (h) [127].

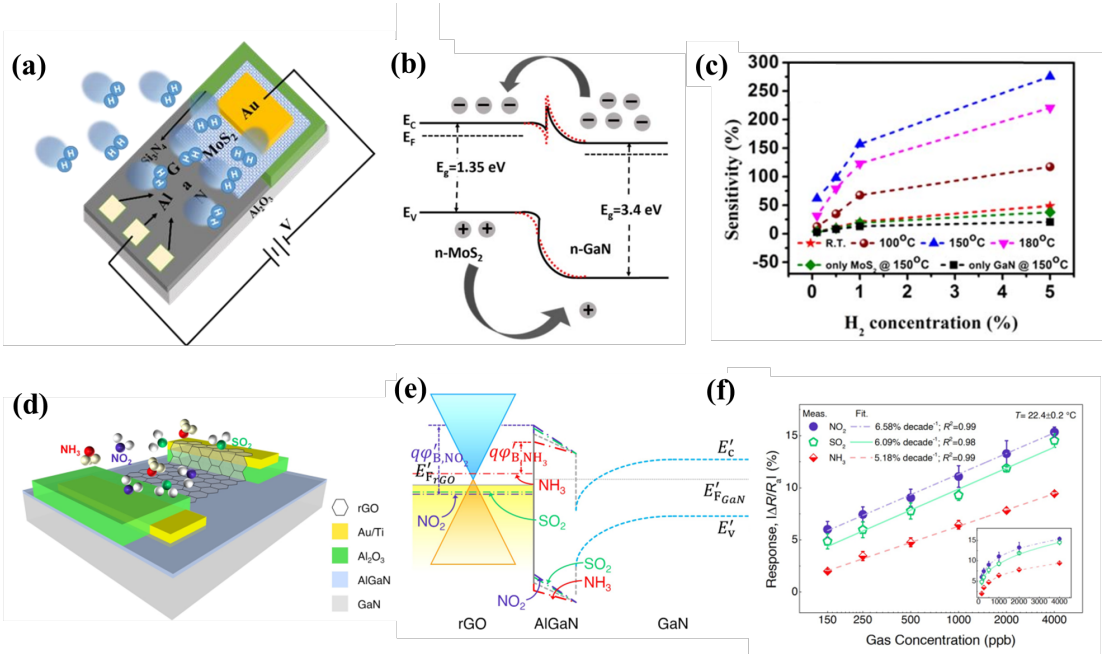

Fig. 9. Gas sensors. (a) Schematic diagram of the MoS_2/GaN gas sensor [144]. (b) The energy band diagram variation of the device in (a) exposure to hydrogen under reverse bias. (c) Sensitivity as a function of hydrogen concentration at different values of temperature of the device in (a). (d) Schematic diagram of rGO/AlGaN/GaN gas sensor [149]. (e) Schematic energy-band diagram variation of the device in (d) exposure to NO_2, NH_3 and SO_2 gases under forward bias condition. (f) Gas concentration dependents of the sensor responses on log and linear (inset) scales.

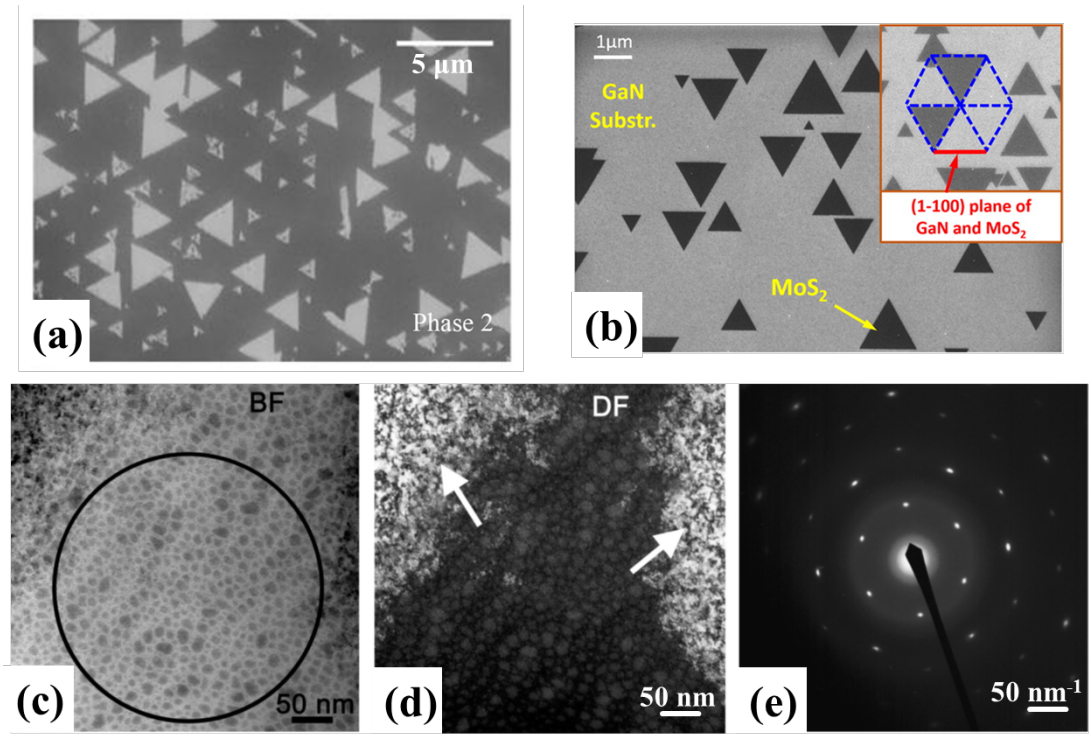

Fig. 10. Morphology of 2D materials in hybrid heterostructures. (a) SEM image of $MoSe_2$ layers on GaN, scale bar: 5 µm [40]. (b) SEM of MoS_2 monolayer triangles on GaN epitaxial crystal, scale bar: 1 µm [38]. TEM image of MoS_2 grown on GaN/AlGaN/GaN (c) bright field, scale bar: 50 nm, (d) dark field, scale bar: 50 nm, (e) select area electron diffraction (SAED) pattern, scale bar: 50 nm^{-1}, [50].